ELEMENTA
Science of the Anthropocene

Jones, EM, et al. 2020. Seasonal dynamics of carbonate chemistry, nutrients and CO_2 uptake in a sub-Arctic fjord. *Elem Sci Anth*, 8: 41. DOI: https://doi.org/10.1525/elementa.438

RESEARCH ARTICLE

Seasonal dynamics of carbonate chemistry, nutrients and CO_2 uptake in a sub-Arctic fjord

Elizabeth M. Jones*, Angelika H. H. Renner*, Melissa Chierici*, Ingrid Wiedmann†, Helene Hodal Lødemel* and Martin Biuw*

Environmental change can have a significant impact on biogeochemical cycles at high latitudes and be particularly important in ecologically valuable fjord ecosystems. Seasonality in biogeochemical cycling in a sub-Arctic fjord of northern Norway (Kaldfjorden) was investigated from October 2016 to September 2018. Monthly changes in total inorganic carbon (C_T), alkalinity (A_T), major nutrients and calcium carbonate saturation (Ω) were driven by freshwater discharge, biological production and mixing with subsurface carbon-rich coastal water. Stable oxygen isotope ratios indicated that meteoric water (snow melt, river runoff, precipitation) had stratified and freshened surface waters, contributing to 81% of the monthly C_T deficit in the surface layer. The timing and magnitude of freshwater inputs played an important role in Ω variability, reducing A_T and C_T by dilution. This dilution effect was strongly counteracted by the opposing effect of primary production that dominated surface water Ω seasonality. The spring phytoplankton bloom rapidly depleted nitrate and C_T to drive highest Ω (~2.3) in surface waters. Calcification reduced A_T and C_T, which accounted for 21% of the monthly decrease in Ω during a coccolithophore bloom. Freshwater runoff contributed C_T, A_T and silicates of terrestrial origin to the fjord. Lowest surface water Ω (~1.6) resulted from organic matter remineralisation and mixing into subsurface water during winter and spring. Surface waters were undersaturated with respect to atmospheric CO_2, resulting in modest uptake of −0.32 ± 0.03 mol C m^{-2} yr^{-1}. Net community production estimated from carbon drawdown was 14 ± 2 g C m^{-2} yr^{-1} during the productive season. Kaldfjorden currently functions as an atmospheric CO_2 sink of 3.9 ± 0.3 g C m^{-2} yr^{-1}. Time-series data are vital to better understand the processes and natural variability affecting biogeochemical cycling in dynamic coastal regions and thus better predict the impact of future changes on important fjord ecosystems.

Keywords: Carbonate chemistry; Ocean acidification; Nutrient cycling; Net community production; Sub-Arctic fjord; Norway

Introduction

Coastal oceans and marine shelves are regions of enhanced uptake of atmospheric carbon dioxide (CO_2) and disproportionately large fraction of primary productivity relative to their areal coverage (Thomas et al., 2004; Borges et al., 2005; Thomas et al., 2009; Cai, 2011). This biological productivity is fuelled by oceanic, atmospheric, and terrestrial nutrient inputs that drive biogeochemical exchanges between the coastal and open ocean and enhanced burial of organic and inorganic carbon (Thomas et al., 2004; Chen and Borges, 2009). Observations in high latitude fjord and coastal regions have shown these regions to be predominantly sinks for atmospheric CO_2, despite large regional variability (Omar et al., 2005; Else et al., 2008b; Signorini et al., 2013; Fransson et al., 2014; Evans et al., 2015; Omar et al., 2016; Yasunaka et al., 2016; Ericson et al., 2018). Mid- and low-latitude coastal regions were thought to be predominantly oceanic CO_2 sources, owing to higher water temperatures and organic matter inputs (Borges et al., 2005; Cai et al., 2006; Chavez et al., 2007; Chen and Borges, 2009). However, increased observations and the development of high-resolution regional models have enabled better resolution of carbon cycling in these regions and identified areas of annual CO_2 uptake in the coastal ocean (Takahashi et al., 2009; Laruelle et al., 2014; Bourgeois et al., 2016; Fennel et al., 2019). Seasonal dynamics are more variable and typically amplified, with temporal changes occurring faster, in the coastal ocean compared to open ocean environments. The processes controlling the biogeochemical cycling in coastal systems are difficult to determine without sustained seasonal measurements of the hydrographic, biogeochemical and metrological variables (Borges et al., 2005; Bozec et al., 2006). Recent research efforts have significantly improved the understanding and quantification of carbon cycling

* Institute of Marine Research, Tromsø, NO
† UiT – The Arctic University of Norway, Tromsø, NO
Corresponding author: Elizabeth M. Jones (elizabeth.jones@hi.no)

in the coastal ocean, e,g, Fennel et al. (2019). However, seasonal baseline estimates of biogeochemical cycling and air–sea CO_2 exchange in some sub-Arctic and Arctic regions are limited. Greater spatial surveys would enable a better understanding of how climate change may affect carbon cycling at high latitudes.

The continental shelf and fjords of the Norwegian coast support a rich food web, cold-water coral reefs, large mammals (whales, seals), seabirds, valuable fish stocks and spawning grounds, and are used for recreation and aquaculture (Matthews and Sands, 1973; Erga and Heimdal, 1984; Salvanes and Noreide, 1993; Fosså et al., 2002; Asplin et al., 2014; Brattegard et al., 2011). The marine environment of the fjords is influenced by water mass circulation, tides, wind regimes, and freshwater inputs. Biogeochemical cycling and primary production exhibit strong seasonality that is controlled by variations in meteorology and hydrography (Eilertsen et al., 1984; Noji et al., 1992; Skarðhamar and Svendsen 2005; Eilertsen and Frantzen, 2007; Eilertsen and Degerlund, 2010; Wiedmann et al., 2016). Steep topography leads to orographic steering of winds, which strongly control mixing and stratification in the fjord (Cottier et al., 2010; Myksvoll et al., 2012), in addition to effects from tides and currents. Persistent down-fjord (to the fjord opening) winds induce upwelling of nutrient-rich coastal water that can stimulate phytoplankton growth in the fjord (Skarðhamar and Svendsen, 2005; Cottier et al., 2010). Up-fjord winds push surface waters coastwards and inhibit the upwelling of subsurface water and create a pressure gradient, which results in pulsed outflow of deep water (Skarðhamar and Svendsen, 2005; Cottier et al., 2010). Katabatic winds descend from the surrounding mountainous regions into the fjord and cool the surface water and enhancing mixing of the water column (Spall et al., 2017). Wind-induced turbulent mixing resuspends detrital and lithogenic material in shallow areas and influences biogeochemical cycling and export fluxes in the water column (Noji et al., 1993; Keck and Wassmann, 1996; Reigstad and Wassmann 1996).

Water column stratification is largely driven by salinity changes from freshwater input and warming/cooling in addition to currents, tides, and winds that drive vertical mixing with saltier subsurface water masses (Inall and Gillibrand, 2010; Cottier et al., 2010). These features influence particle transport, phytoplankton production and biogeochemical cycling (Klinck et al., 1981; Syvitski et al., 1987). The Norwegian Coastal Current transports fresher waters and supplies the fjords with nutrients and oxygen (Aure and Stigebrandt, 1989) to support enhanced primary production and a diversity of marine life (Erga and Heimdal, 1984; Salvanes and Noreide, 1993). From late autumn to winter, cooling, convective mixing and low light levels reduce phytoplankton activity and net respiration by heterotrophic organisms and organic matter remineralisation enriches the water column with inorganic carbon and nutrients (Noji et al., 1993; Eilertsen and Frantzen, 2007; Eilertsen and Dagerlund, 2010). From spring, light availability, stratification, temperature and day length increase with increases in phytoplankton biomass and productivity (Reigstad and Wassmann 1996; Eilertsen and Frantzen, 2007). Autotrophic activity utilises the winter stock of nutrients and drives biological carbon uptake during the growing season. Zooplankton abundance typically peaks during the spring bloom, declines throughout the summer as phytoplankton stocks diminish and often slightly increases during the smaller autumn blooms (Grønvik and Hopkins 1984; Michelsen et al. 2017).

High latitude surface waters are particularly sensitive to increases in atmospheric CO_2 and are likely to be the first areas to experience widespread ocean acidification; i.e., the lowering of pH and carbonate mineral saturation (Ω) states (Orr et al., 2005; Fabry et al., 2009; Doney et al., 2009). This sensitivity is due to the naturally low seawater carbonate ion concentrations as a result of greater freshwater inputs from melting sea ice, glacial meltwater, precipitation and river runoff (Chierici and Fransson, 2009; Fransson et al., 2013; Fransson et al., 2015). Compared to seawater, freshwater sources are low in total alkalinity (A_T), the natural buffer against acidity, and dilute the carbonate ion concentrations in seawater and decrease calcium carbonate (calcite or aragonite, $CaCO_3$) saturation. These processes enhance surface water acidification in coastal and seasonally ice-covered regions (Chierici and Fransson, 2009; Yamamoto-Kawai et al., 2009; Azetsu-Scott et al., 2014; Evans et al., 2014; Reisdorph and Mathis, 2014; Fransson et al., 2015). This enhancement occurs at potentially faster rates than the decreased pH and carbonate concentrations due to anthropogenic CO_2 uptake by the ocean; the impact on fjords will depend on the potential for atmospheric CO_2 uptake, as driven by biological production, and their geochemical buffering capacity to ocean acidification. Ocean acidification impacts the growth, metabolic processes and life cycles of marine organisms, especially those that precipitate $CaCO_3$ to form shells and skeletons (Orr et al., 2005; Fabry et al., 2008). When the calcium carbonate saturation decreases below the equilibrium threshold ($\Omega = 1$) for carbonate precipitation and dissolution in seawater, the potential for $CaCO_3$ to dissolve increases. The rate of acidification in the open ocean of the Norwegian Sea has been well documented with long-term decreases in pH and aragonite saturation state (Lauvset et al., 2015; Jones et al., 2019). Few studies have been carried out to investigate the seasonal biogeochemical cycling and CO_2 uptake in northern Norwegian fjords, in contrast to the numerous studies from other northern fjord systems such as Svalbard (Omar et al., 2005; Fransson et al., 2014; Fransson et al., 2015; Ericson et al., 2019a; 2019b) and Greenland (Rysgaard et al., 2012; Meire et al., 2015).

This study presents the first time-series measurements of carbonate chemistry (dissolved inorganic carbon, C_T, and total alkalinity, A_T), macronutrients (nitrate + nitrite, phosphate, silicate) and $\delta^{18}O$ covering a full annual cycle in a sub-Arctic fjord, Kaldfjorden. The data provide baseline hydrographic and biogeochemical measurements in the full water column during spring, summer, autumn and winter and emphasise the importance of time-series sampling to unravel the processes controlling the seasonal variability of carbon cycling in this region of the coastal ocean. The main objectives of this work were to

(1) investigate the seasonal cycling in carbonate chemistry in the context of physical (freshwater inputs and water mass mixing) and biogeochemical (photosynthesis/respiration, remineralisation, calcification, air–sea fluxes) forcing; (2) estimate net community production (NCP) and annual air–sea CO_2 exchange; and (3) determine the current ocean acidification state.

Methods

Study area

Kaldfjorden (69.75°N, 18.68°E) is an ice-free fjord, 15 km long and about 2 km wide, on the western part of Kvaløya, Tromsø county, northern Norway (**Figure 1**). The fjord has a north–south orientation with a typical structure of U-shaped valley bounded by steep, glacially carved sides and is connected to the north Atlantic Ocean across the Norwegian shelf. Kaldfjorden has a partial sill between 75 and 135 m at the mouth and two basins (150–220 m) separated by a ridge. The seafloor shallows towards the inner part of the fjord. The Kaldfjorden marine environment hosts pelagic and benthic calcifiers, plays a role in seasonal migration of herring and supports aquaculture production of Atlantic salmon (Register of Aquaculture Permissions, 2018). The region experiences the polar night from the end of November to the end of January and 24-hour daylight from the end of May until the end of July. The growing season in northern Norway is typically between the end of March and October/November, with peaks in phytoplankton biomass during the spring bloom in mid/late April and a smaller autumn bloom can occur by the end of August or early September (Eilertsen and Frantzen, 2007).

The hydrography of Kaldfjorden is influenced by the circulation of water masses of coastal and Atlantic origin, mixed with local freshwater. The North Atlantic Current carries warm and saline Atlantic Water ($S > 35$; $5 < T \leq 10$°C) northwards along the Norwegian continental slope (Skarðhamar and Svendsen, 2005). The Norwegian Coastal Current carries colder and less saline Norwegian Coastal Water ($S < 35$; $4 < T \leq 12$°C) along the continental shelf (Saetre, 2007), which is freshened by riverine inputs (Nordby et al., 1999; Skarðhamar and Svendsen, 2005; Albretsen et al., 2012). Winter Mode Water is formed from cooling and convective mixing of the local fjord water during wintertime. Several small streams transport freshwater (terrestrial snow and ice melt, precipitation) into the fjord.

Meteorological observations

Time-series measurements of precipitation, air temperature and wind speeds were recorded at an hourly resolution by the Norwegian Meteorological Institute (www.eKlima.met.no) at the Tromsø observation site (**Figure 2**). Wind speeds recorded at Tromsø are a better proxy for conditions in Kaldfjorden as the orientation is very similar for both sites and orographic effects will therefore be similar; wind data at other proximal sites at Maasvik and Hekkingen fyr showed more dramatic orographic effects. Data are freely available and were retrieved on 13 September 2018.

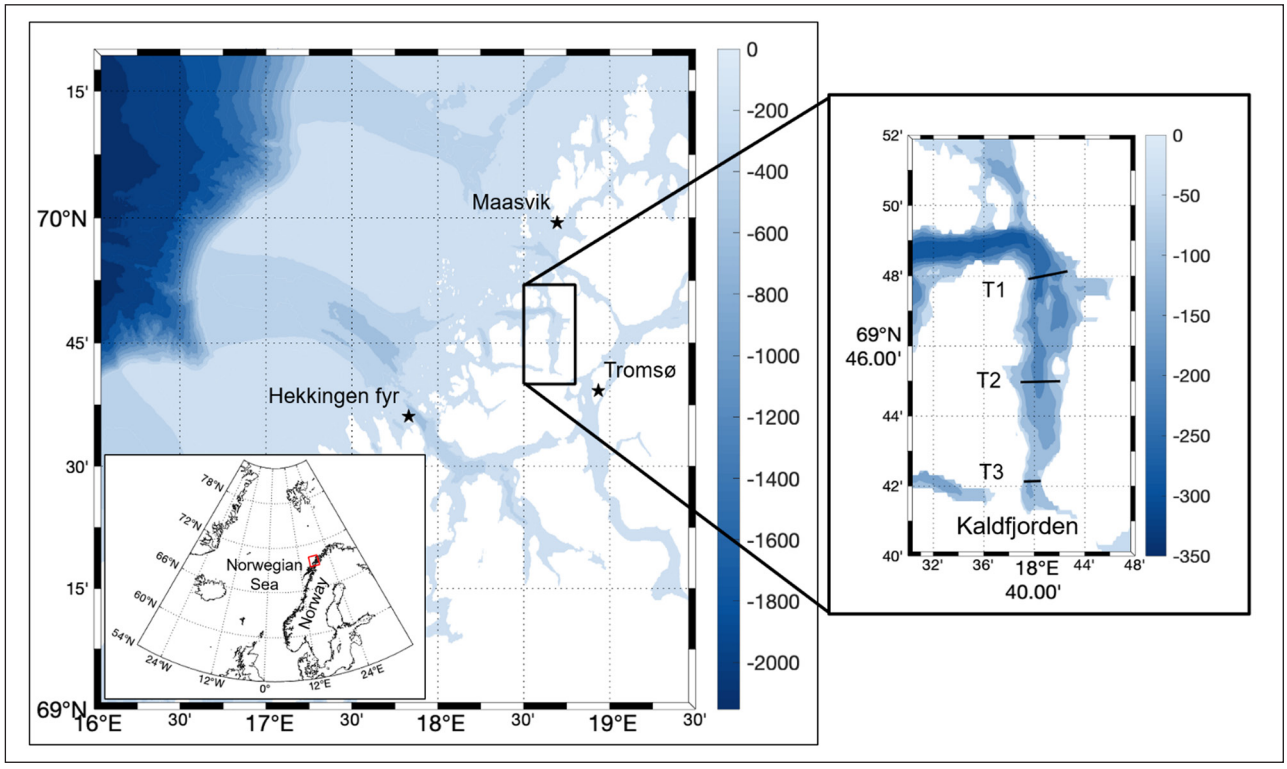

Figure 1: Map of the study region in northern Norway. Left: overview of the bathymetry of the shelf off Tromsø with the location of Kaldfjorden marked by the black rectangle. The nearest weather stations are marked by black stars and the inset shows the location in northern Norway. Right: Kaldfjorden and the location of the hydrographic transects (T1, T2, T3). Bathymetric data (depth, m) were provided by the Norwegian Mapping Authority at http://www.kartverket.no. DOI: https://doi.org/10.1525/elementa.438.f1

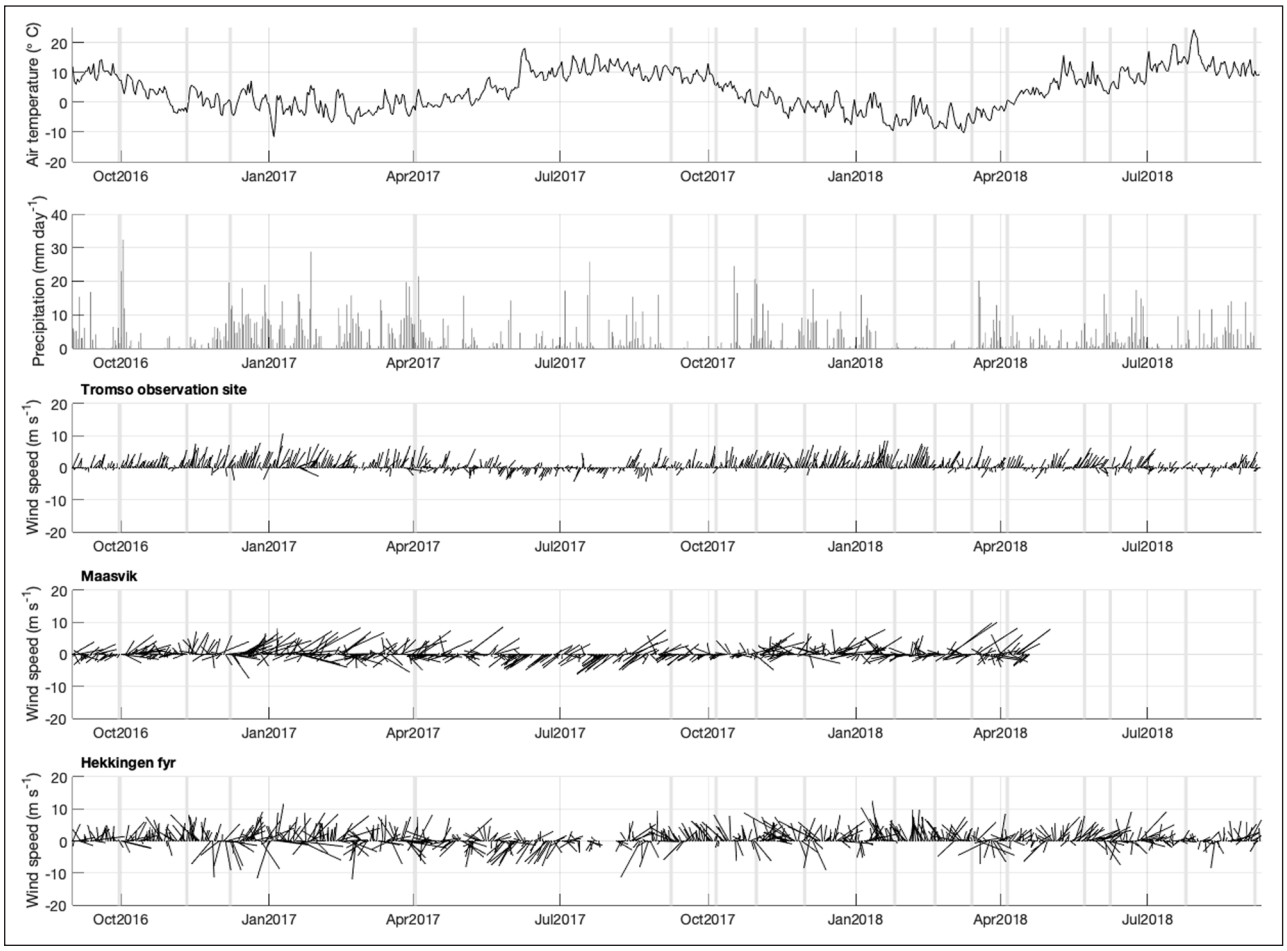

Figure 2: Time series of meteorology at stations near Kaldfjorden. Top panel: 24-hour average air temperature (°C). Second panel: precipitation per 24 hour (mm day^{-1}). Third panel: wind vectors (m s^{-1}) for Tromsø observation site. Forth panel: wind vectors (m s^{-1}) for Maasvik. Fifth panel: wind vectors (m s^{-1}) for Hekkingen fyr. All wind vectors are daily averages and point in the direction the wind was blowing towards. Times of sampling of hydrographic measurements are indicated by grey vertical lines. DOI: https://doi.org/10.1525/elementa.438.f2

Hydrographic measurements

Hydrographic measurements and water samples were obtained along three transects across the outer (T1), middle (T2) and inner (T3) parts of Kaldfjorden from small motorboats or larger research vessels (**Table 1**). Vertical conductivity-temperature-depth (CTD) profiles were obtained east–west along each of the transects at near-monthly resolution from November 2016 to July 2018. On small boats, a handheld CTD (SAIV SD208) was used. On research vessels, onboard Seabird Electronics SBE911+ were used. Onboard RV *Johan Ruud* and on the small boats, water sampling was carried out using a single Niskin bottle mounted above the CTD. The bottle was lowered several times per station to each sampling depth. On the larger research vessels, a CTD rosette with 12 Niskin bottles attached was available, and all samples were taken on the upcast of the CTD profile. **Table 1** summarizes details of the sampling, vessels and CTD sensors that were used during this study. The SAIV CTD #1321 used from September 2017 until September 2018 was calibrated in summer 2017. When possible, the SAIV CTD was deployed simultaneously with the SBE CTD frame for calibration and intercomparison of the sensors. Castaway CTD sensors were used as further indicators for potential differences between the SAIV CTDs. All Seabird CTD sensors are factory-calibrated annually and the conductivity cells are further calibrated against salinity samples throughout the year. All CTD data were averaged into 1-dbar pressure bins, and the upcasts of the CTD were used for analyses due to more stable vertical speed during recovery. Salinity data are reported on the Practical Salinity Scale.

Freshwater fractions (FW) were determined using the in situ salinity (S) relative to the mean salinity (34.17 ± 0.24; S_{ref}) of Norwegian Coastal Water (Equation 1), as measured below 200 m at the outer fjord (T1) during the study period:

$$FW = \frac{S_{ref} - S}{S_{ref}} \quad (1)$$

Water sampling and analysis

Biogeochemical water samples were taken from the central hydrographic station on each transect (T1, T2, T3) from 3–6 depths in the water column, typically at the surface (0–5 m), 25 m, 50 m, 70 m, 100 m, 150 m, and bottom, depending on the water column depth, which was 230 m (T1), 175 m (T2) and 115 m (T3). Samples for carbonate

Table 1: Sampling event date, CTD type, water sampling details and vessels used. DOI: https://doi.org/10.1525/elementa.438.t1

Date (dd.mm.yyyy)	Vessel	CTD	Bottle/rosette	Water samples taken		
				C_T/A_T	Nutrients	$\delta^{18}O$
30.09 and 10.10.2016	M/V *Chinga*	SAIV SD208 #1192	bottle	x	x	x
11 and 14.11.2016	M/V *Chinga*	SAIV SD204 #866 Castaway CC1512008	bottle	x	x	x
30.11 and 08.12.2016	M/V *Chinga*	SAIV SD208 #1141 Castaway CC1512008	–[a]	–	–	–
02.04.2017	R/V *Helmer Hanssen*	SBE911plus	rosette	x	x	x
05 and 08.09.2017	M/V *Chinga*	SAIV SD208 #1321	bottle	x	x	x
05 and 06.10.2017	M/V *Chinga*	SAIV SD208 #1321 Castaway CC1509012	bottle	x	x	x
31.10.2017	R/V *Helmer Hanssen*	SBE911plus	rosette	x	x	x
30.11–02.12.2017	R/V *Johan Hjort*	SBE911plus	rosette	x	x	x
22–25.01.2018	M/V *Dytiscus*	SAIV SD208 #1321 Castaway CC1509012	bottle	x	x	x
19.02.2018	M/V *Dytiscus*	SAIV SD208 #1321	–	–	–	–
13 and 14.03.2018	R/V *Johan Ruud*	SAIV SD208 #1321 SBE911plus	bottle	x	x	x
04–06.04.2018	R/V *Helmer Hanssen*	SAIV SD208 #1321 SBE911plus	rosette	x	x	x
22 and 23.05.2018	M/V *Dytiscus*	SAIV SD208 #1321 Castaway CC1509012	bottle	x	x	x
08.06.2018	M/V *Dytiscus*	SAIV SD208 #1321	bottle	x	x	x
19 and 25.07.2018	R/V *Kronprins Haakon*, F/V *Kjell-Arne*	SAIV SD208 #1321 SBE911plus	bottle/rosette	x	x	x
06.09.2018	S/V *Verona*	SAIV SD208 #1321	bottle	x	x	x

[a] Water samples not taken.

chemistry were drawn from the Niskin bottle via a silicon tube into 250-mL borosilicate bottles, preserved with saturated mercuric chloride (60 μL) and stored in the dark at 4°C. Analyses for total dissolved inorganic carbon (C_T) and total alkalinity (A_T) were carried out at the Institute of Marine Research in Tromsø, Norway, within 6 months. Following methods outlined in Dickson et al. (2007), C_T was determined using gas extraction of acidified (8.5% H_3PO_4) samples followed by coulometric titration and photometric detection (Johnson et al., 1987) using a Versatile Instrument for the Determination of Titration carbonate (VINDTA 3D, Marianda, Germany). The determination of A_T was carried out by potentiometric titration with 0.1 M hydrochloric acid in a semi-open cell using a Versatile Instrument for the Determination of Titration Alkalinity (VINDTA 3S, Marianda, Germany). The average standard deviation for C_T and A_T, determined from replicate sample analyses, was within ± 2 μmol kg^{-1}. Measurements were calibrated against Certified Reference Materials (CRM, provided by A. G. Dickson, Scripps Institution of Oceanography, USA).

Samples for macronutrients nitrate + nitrite ($NO_3 + NO_2$), nitrite (NO_2), phosphate (PO_4) and silicic acid ($Si[OH_4]$) were collected from the Niskin bottles into 20-mL vials, preserved with chloroform and stored at 4°C. Analysis was carried out at the Institute of Marine Research, Bergen, Norway, using a Flow Solution IV analyzer from O.I. Analytical, United States, following Grasshoff et al. (2009). The analyser was calibrated using reference seawater from Ocean Scientific International Ltd., United Kingdom. The semi-conservative tracer N* ($[NO_3 + NO_2] - 16[PO_4]$; Gruber and Sarmiento, 1997) was used to identify anomalies of nitrate + nitrite relative to phosphate, compared to global averages. As such, N* indicates periods of nitrogen replenishment or loss, as negative values suggest nitrogen deficits due to denitrification and positive values suggest nitrogen excess due to nitrogen fixation. However, these changes also include signals of advection of different water masses with different nutrient signatures.

Samples for determination of the ratio of the stable oxygen isotope of seawater ($\delta^{18}O$) were transferred into 20-mL vials and stored in the dark at 4°C until analysis using a Thermo Fisher Scientific Delta V Advantage mass spectrometer with Gasbench II. Data were standardised relative to Vienna Standard Mean Ocean Water (VSMOW) for $\delta^{18}O$ (‰) with a reproducibility of replicate analyses of ±0.04‰.

Carbonate system determinations

Calcium carbonate saturation and surface water fCO_2

Calcium carbonate ($CaCO_3$) saturation state (Ω) for the biomineral aragonite and the surface water fugacity of CO_2 (fCO_2) were determined from C_T and A_T, and in situ temperature, salinity, pressure and macronutrient concentrations using the CO_2 system program CO2SYS (Lewis and Wallace, 1998; van Heuven, 2011). The carbonic acid dissociation constants (pK_1 and pK_2) of Mehrbach et al. (1973) as refit by Dickson and Millero (1987) were selected, as they have shown good agreement between measured and calculated values in Arctic waters (Chen et al., 2015; Woosley et al., 2017) and were selected for similar studies in sub-Arctic/Arctic regions (Chierici et al., 2019; Ericson et al., 2019). Ω is used as an indicator for changes in carbonate chemistry in relation to ocean acidification. When $\Omega < 1$, waters are undersaturated with respect to $CaCO_3$ and thus minerals are sensitive to dissolution.

Variability in surface water fCO_2 can be partitioned into temperature and biological signals by applying a temperature normalisation to the average surface water temperature (T_{ave}, 7.51 ± 3.17°C, n = 49) for all seasons (Takahashi et al., 2002):

$$fCO_{2\,T} = fCO_2 \cdot \exp 0.0423 \cdot (T_{ave} - T_{obs}) \quad (2)$$

where $fCO_{2\,T}$ (**Equation 2**) is normalised fCO_2 and T_{obs} is the temperature corresponding to the surface water fCO_2. The remaining fCO_2 variability is attributed to changes in C_T (assuming constant A_T) due to biological processes. This approach does not account for variations in C_T from other processes including A_T, riverine inputs, sediment fluxes and air–sea CO_2 exchange; these variations are incorporated into the biological signal.

Air–sea CO_2 fluxes

The potential for air–sea CO_2 exchange is determined by the difference between CO_2 in the sea and overlying air. Fluxes of CO_2 (Equation 3) were calculated from the quasi-monthly air–sea gradient in fCO_2 (ΔfCO_2), the solubility coefficient of CO_2 (K_0) from Weiss (1974) and the gas transfer coefficient (K) which is a function of wind speed (Wanninkhof, 2014):

$$CO_2 flux = k \cdot K_0 \cdot \Delta fCO_2 \quad (3)$$

The uncertainty in the parameterization of the gas transfer velocity k was taken as 20% (Wanninkhof, 2014). The ΔfCO_2 is the difference between the calculated fCO_2 in surface seawater and the daily mean air fCO_2 value as determined from atmospheric CO_2 values. Atmospheric CO_2 data were obtained as mixing ratios (xCO_2) at hourly resolution at the Sammaltunturi observation site in Pallas, northern Finland (67.9736°N, 24.1158°E), operated by the Finnish Meteorological Institute (FMI). Data were accessed via the World Data Centre for Greenhouse Gases on 5 October 2019. Daily atmospheric CO_2 concentrations were averaged into monthly means and converted to partial pressures, using the mean monthly air pressures and the seawater vapor pressure as determined from seawater salinity and temperature of the surface waters (Ambrose and Lawrenson, 1972; Millero and Leung, 1976). The average fCO_2 in dry air was 397 ± 9 µatm (n = 46) during the study period (30 September 2016 to 06 September 2018). Negative values of ΔfCO_2 and CO_2 flux indicate surface water CO_2 undersaturation and uptake of atmospheric CO_2. The uncertainty in the atmospheric CO_2 concentrations is estimated as ±6 ppm as the maximum standard deviation of monthly means from daily concentrations, and the CO_2 flux uncertainty is estimated as ±0.1 mmol m^{-2} day^{-1}. Wind speed data were averaged into monthly means and corrected to 10 m above sea level (Hartman and Hammond, 1985). The uncertainty in the wind speed data is estimated as ±10 m s^{-1} as the root mean square error of one standard deviation per monthly mean from hourly observations. Air–sea CO_2 exchange per month was estimated from the daily CO_2 flux calculated for each (quasi-monthly) sampling event multiplied by the number in the respective sampling month.

Marine carbonate system

The temporal evolution of C_T in the upper 50 m was determined from the quasi-monthly changes of C_T (**Equation 4**) during the full annual cycle in 2017–2018. The 0–50 m depth range was selected to encompass the seasonal mixed layer, and changes were determined by integrating from the surface to 50-m depth. The total change in C_T ($\Delta C_{T\,total}$) is determined from the main processes that influence seawater C_T: salinity changes ($\Delta C_{T\,sal}$), mixing with subsurface water ($\Delta C_{T\,mix}$), photosynthesis/respiration ($\Delta C_{T\,bio}$), air–sea CO_2 exchange ($\Delta C_{T\,flux}$) and calcium carbonate formation/dissolution ($\Delta C_{T\,CaCO_3}$):

$$\Delta C_{T\,total} = \Delta C_{T\,sal} + \Delta C_{T\,mix} + \Delta C_{T\,bio} + \Delta C_{T\,flux} + \Delta C_{T\,CaCO_3} \quad (4)$$

where $\Delta C_{T\,sal}$ is determined from the difference between the total monthly C_T change and the change in salinity-normalised C_T. Salinity normalisation using the traditional method (Equation 5) removes effects of dilution/enrichment, where variable (X) measured at in situ salinity (S) was salinity-normalised (X_{sal}) to the subsurface Norwegian Coastal Water salinity reference (34.17; as described above) following Friis et al. (2003):

$$X_{sal} = \frac{X}{S} \cdot S_{ref} \quad (5)$$

From the C_T-salinity and C_T-$\delta^{18}O$ relationships, values of C_T at zero salinity were estimated at -696 µmol kg^{-1} and 651 µmol kg^{-1}, respectively (see section on *Seasonality in freshwater and deep-water effects*). The negative and positive estimates yield different interpretations of the freshwater endmember and the resultant $C_{T\,sal}$ values, which are dependent upon the salinity normalisation method used (Friis et al., 2003). Therefore, in consideration of the significant difference in C_T endmember estimates, with respect to the sign of the value, and following the normalisation of inorganic nutrient data (with Equation 5), the C_T data were normalised using the traditional method, further

discussed below (see section on **Uncertainty assessment**). $\Delta C_{T\,sal}$ integrates the signal from salinity changes due to freshwater inputs (decreased C_T and A_T) and advection of different water masses. $\Delta C_{T\,mix}$ was estimated from monthly changes in the mixed layer (inferred from changes in potential density) and the difference between the average C_T in the upper 50 m and the average C_T in the subsurface Norwegian Coastal Water (2137 ± 13 μmol kg^{-1}, n = 15). Here a deepening of the mixed layer (increased potential density) infers vertical mixing and increased C_T, adapted from Chierici et al. (2011). $\Delta C_{T\,mix} = 0$ if there is no change or a shallowing of the mixed layer and integrates the signal from potential density increases (increased C_T and A_T) due to vertical mixing between sampling events.

Monthly changes in C_T due to photosynthetic fixation of C_T and production of organic carbon ($\Delta C_{T\,bio}$) were determined by (1) using monthly changes in salinity-normalised nitrate and the C/N Redfield ratio of 6.6 (Redfield et al., 1963) to estimate C_T uptake ($\Delta C_{T\,bio\,N}$) and by (2) residual difference between the total C_T change and the sum of all other contributing factors ($\Delta C_{T\,bio\,C}$). These estimates yield the net community production (NCP), which describes the net primary production minus heterotrophic respiration. $\Delta C_{T\,bio}$ is negative when respiration exceeds photosynthesis, thus the reverse transformation recycles organic carbon back into its inorganic form. $\Delta C_{T\,flux}$ is determined from the air–sea CO_2 flux estimated at the time of each sampling event (quasi-monthly), multiplied by the number of days per respective sampling month. Changes in the ΔfCO_2 and wind speed are assumed to be linear (or the net result between positive and negative fluctuations) between each quasi-monthly sampling event. Negative fluxes indicate CO_2 undersaturation in surface water and atmospheric CO_2 uptake and thus yield a positive $\Delta C_{T\,flux}$, i.e., input of C_T to the surface water. $\Delta C_{T\,CaCO_3}$ accounts for changes in A_T that influence C_T, as outlined below.

Following the approach for C_T, monthly A_T changes were determined (Equation 6) from contributions due to salinity changes ($\Delta A_{T\,sal}$), mixing ($\Delta A_{T\,mix}$), a minor contribution from photosynthesis/respiration ($\Delta A_{T\,bio}$) and calcium carbonate ($CaCO_3$) formation/dissolution ($\Delta A_{T\,CaCO_3}$), which likely includes terrestrial/benthic fluxes:

$$\Delta A_{T\,total} = \Delta A_{T\,sal} + \Delta A_{T\,mix} + \Delta A_{T\,bio} + \Delta A_{T\,CaCO_3} \quad (6)$$

Changes in A_T due to salinity variations ($\Delta A_{T\,sal}$) were determined using the salinity normalisation method that accounts for a non-zero freshwater endmember (Friis et al., 2003), with A_T of 337 μmol kg^{-1} determined from linear regression analysis with $S = 0$ from the A_T-salinity relationship (presented in the section on *Seasonality in freshwater and deep-water effects*). $\Delta A_{T\,mix}$ was estimated as described for $\Delta C_{T\,mix}$ using an average A_T in the subsurface Norwegian Coastal Water (2282 ± 10 μmol kg^{-1}). Changes in A_T associated with the uptake and release of nitrate during photosynthesis/respiration ($\Delta A_{T\,bio}$) can be estimated as one unit of NO_3 uptake increases A_T by one unit, therefore $\Delta A_{T\,bio} = -0.15\,\Delta C_{T\,bio}$ (Brewer and Goldman, 1976). Changes in A_T due to $CaCO_3$ formation/dissolution ($\Delta A_{T\,CaCO_3}$) are estimated by considering the potential alkalinity (A_T*); the sum of salinity-normalised A_T and NO_3 (Brewer and Goldman, 1976). Thus, $\Delta C_{T\,CaCO_3} = \frac{1}{2}(\Delta A_{T\,CaCO_3})$, which accounts for carbonate mineral precipitation and dissolution (Zeebe and Wolf-Gladrow, 2001). The $\Delta A_{T\,CaCO_3}$ term is also likely to include any terrestrial and sediment/benthic carbonate fluxes.

Monthly ΔC_T and ΔA_T were used to determine the corresponding changes in $\Delta\Omega$ for aragonite ($\Delta\Omega$ aragonite). For each process (salinity changes, mixing, photosynthesis/respiration, air–sea CO_2 exchange, calcium carbonate formation/dissolution) the associated ΔC_T and ΔA_T was added to the C_T and A_T of the previous sampling event with in situ temperature, salinity and macronutrient concentrations in the surface layer. The CO2SYS program was then used to calculate the perturbed Ω to yield monthly estimates of changes in surface water Ω from the key contributing processes: $\Delta\Omega_{sal}$, $\Delta\Omega_{mix}$, $\Delta\Omega_{bio}$, $\Delta\Omega_{flux}$ and $\Delta\Omega_{CaCO_3}$.

Uncertainty assessment

Uncertainties in the determined effects of the physical and biogeochemical processes on ΔC_T, ΔA_T and $\Delta\Omega$ were estimated as follows. Errors associated with monthly $\Delta C_{T\,total}$ and $\Delta A_{T\,total}$ were estimated to be ±0.2 mol m^{-2} based on analytical precision of C_T and A_T (±2 μmol kg^{-1}). Uncertainties in $\Delta C_{T\,sal}$ and $\Delta A_{T\,sal}$ were estimated by consideration of the different normalisation methods that were applied (see section on **Marine carbonate system**). For the A_T endmember of 337 μmol kg^{-1}, the difference between salinity normalised and measured A_T ranged between −23 μmol kg^{-1} and 131 μmol kg^{-1}. For the 1340 μmol kg^{-1} endmember, the differences varied from −11 μmol kg^{-1} to 58 μmol kg^{-1}. Thus, the salinity-derived (lower) endmember value yields a greater correction to the A_T values. For C_T and the traditional normalisation method, the difference between $C_{T\,sal}$ and C_T ranged between −25 μmol kg^{-1} and 143 μmol kg^{-1}. Using the 651 μmol kg^{-1} endmember and the non-zero freshwater endmember normalisation, the differences were from −17 μmol kg^{-1} to 95 μmol kg^{-1}. The upper bound of the $A_{T\,sal}$ uncertainty can be considered as the maximum difference between the $A_{T\,sal}$ values from each endmember, i.e., 131–58 μmol kg^{-1}, which is 73 μmol kg^{-1}. Similarly, the uncertainty in the $C_{T\,sal}$ is estimated as 48 μmol kg^{-1}. Therefore, the upper bound of the $\Delta A_{T\,sal}$ and $\Delta C_{T\,sal}$ uncertainty (maximum difference between $\Delta A_{T\,sal}$ and $\Delta C_{T\,sal}$ for the two normalisation methods used for each) is 1.75 mol m^{-2} month^{-1} and 1.14 mol m^{-2} month^{-1}, respectively. Using the traditional normalisation technique likely over-corrects $C_{T\,sal}$, as explained in Friis et al. (2003); however, the uncertainty is less compared to that estimated for the $A_{T\,sal}$ methods, and therefore the standard normalisation method is considered suitable for the inorganic carbon (and nutrient) data in this study. Uncertainties in $\Delta C_{T\,mix}$ and $\Delta A_{T\,mix}$ were estimated to be ±0.4 mol m^{-2} based on analytical precision of C_T and A_T (±2 μmol kg^{-1}). Uncertainties in $\Delta C_{T\,bio\,N}$ and $\Delta A_{T\,bio\,N}$ were estimated as ±0.1 mol m^{-2} from the analytical precision of NO_3 of ±3% and the uncertainty in the C/N ratio, which was set to ±1 μmol kg^{-1} to account for variations in the ratio from 6.6 (Redfield et al., 1963) to 6.7 (Frigstad et al., 2014). The uncertainties in $\Delta A_{T\,CaCO_3}$ and $\Delta C_{T\,CaCO_3}$ were estimated as

±0.2 and ±0.1 mol m^{-2}, respectively, from the analytical precision of NO_3 (±3%) and A_T (±2 µmol kg^{-1}).

Uncertainties in the calculated surface water fCO_2 (xCO_2) result from uncertainties in C_T, A_T, salinity, temperature, *K*1 and *K*2 that were added to each value of each property and used as inputs in CO2SYS to yield an upper bound error as ±9 µatm (±9 ppm). Based on a max value for *k* of 2.3, the associated error (20%; Wanninkhof, 2014) for *k* is ±0.46, thereby the uncertainty for $\Delta C_{T\ flux}$ is estimated as ±0.01 mol m^{-2}. Uncertainties in $\Delta C_{T\ bio\ C}$ and $\Delta A_{T\ bio\ C}$ are estimated as ±1.1 mol m^{-2} from the sum of all associated uncertainties for each contributing term. Following the same approach, errors associated with $\Delta\Omega_{total}$ were estimated to be ±0.08 based on uncertainties of Ω ± 0.04 from the input parameters run through CO2SYS. Using the associated errors for each ΔC_T and ΔA_T term in CO2SYS, uncertainties for ΔΩ were determined as $\Delta\Omega_{sal}$ ± 0.12, $\Delta\Omega_{mix}$ ± 0.12, $\Delta\Omega_{bio\ N}$ ± 0.08, $\Delta\Omega_{flux}$ ± 0.02, $\Delta\Omega_{CaCO3}$ ± 0.09 and $\Delta\Omega_{bio\ C}$ ± 0.43.

Results

Meteorology

Air pressure was stable during the summer and more variable for the rest of the year. Air temperatures were warmest (>20°C) in June, July and August and coldest (<–10°C) from January to March (**Figure 2**). Average daily precipitation was 2.7 ± 4.7 mm (n = 706), with intense events (10–32 mm day^{-1}) occurring sporadically throughout the year. Wind data measured every 6 hours showed that the average and the most frequent wind direction were 175 ± 90° (n = 2826) and 194°, respectively, which shows the impact of orographic effects at the Tromsø site. The prevailing southerly winds in Tromsø indicate that up-fjord (from the inner to outer part of the fjord) winds likely prevailed in Kaldfjorden. Wind speeds were on average 3.3 ± 2.1 m s^{-1} (n = 2826), ranging from calm periods to strong gusts (up to 12.9 m s^{-1}). High pressure systems at the end of September and early October 2017 and February was accompanied by elevated temperatures and low rainfall. Winter storms (in December and January) were characterised by increased wind speeds, warmer air, and precipitation. June 2018 was a notably wet month relatively to the rest of the year. July 2018 had the warmest air temperatures (25–28°C) and very low precipitation as a result of higher and stable air pressure. Surface water temperatures were at the seasonal maximum during this period.

Hydrography

The water column was strongly stratified across Kaldfjorden from June to October (**Figure 3**). Highest potential temperatures (θ up to 12.27°C) were found in the upper 50 m from June to October 2017 and 2018 (**Figure 4**). Lower salinity (*S* ~ 32) water occupied the upper 20 m during this period (**Figure 5**). Subsequent cooling and convective mixing eroded the stratification in November and the water column was well mixed from December until May. During periods of weak stratification, the effects of tides are likely greater across the region (Skarðhamar and Svendsen, 2005). The fjord water resembled a modified variety of Norwegian Coastal Water ($S < 34.8$, $4 < \theta \leq 12$°C; Nordby et al., 1999) with local effects of cooling, warming and freshening (**Figure 6**). The pycnocline persisted from May until November with modified Norwegian Coastal Water as the warmer and saltier watermass below 100 m. In the outer part of the fjord (T1), subsurface coastal water

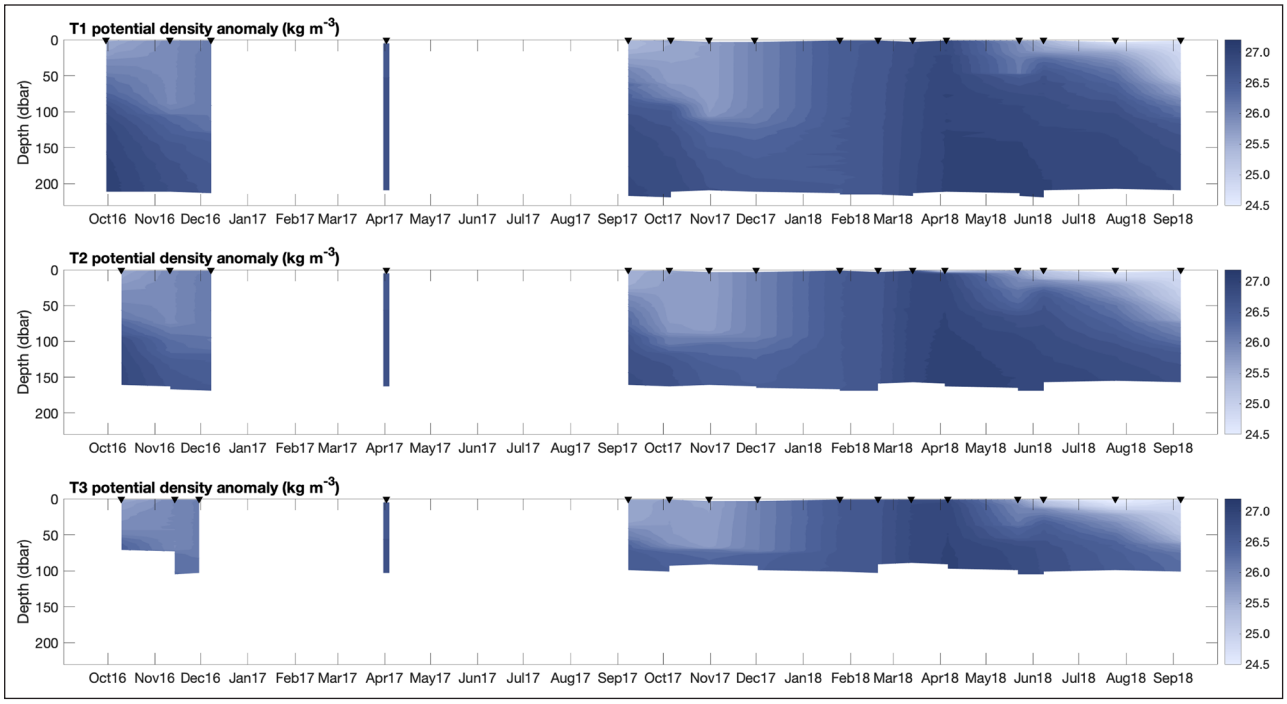

Figure 3: Time series of seawater potential density anomaly from October 2016 to September 2018. Measurements of seawater potential density anomaly (kg m^{-3}; color scale bar) from CTD deployments at the central hydrographic station of the outer (T1), middle (T2), and inner (T3) transects. Sampling events are indicated by black triangles. DOI: https://doi.org/10.1525/elementa.438.f3

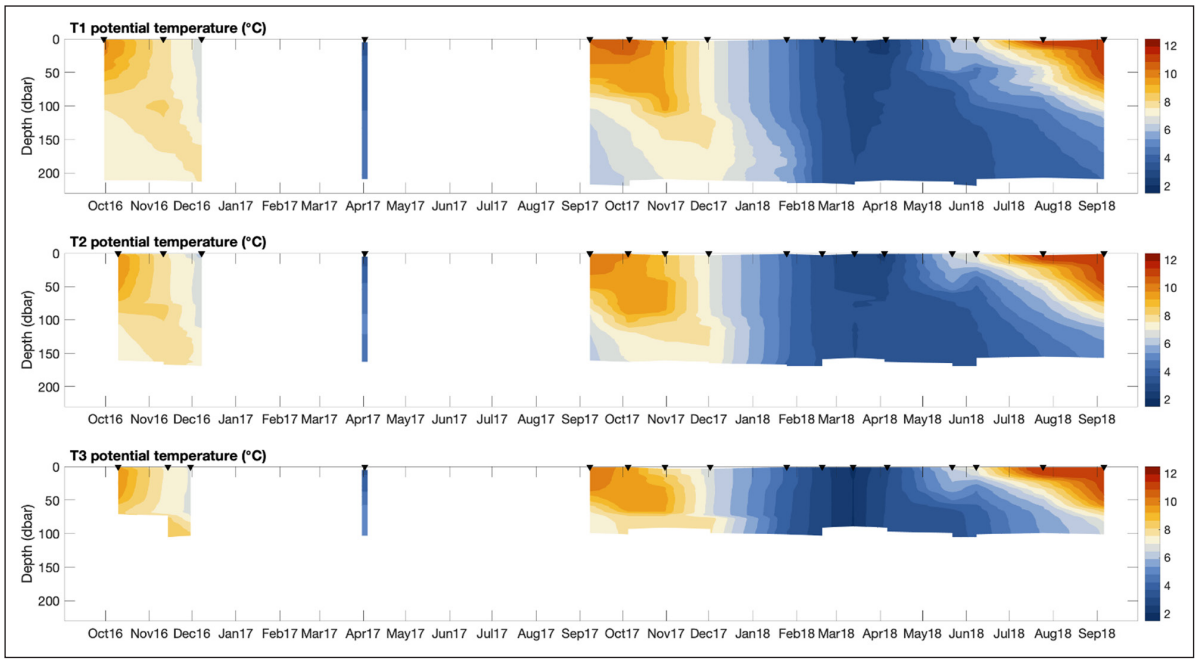

Figure 4: Time series of seawater temperature from October 2016 to September 2018. Seawater potential temperature (°C, color scale bar) from CTD deployments at the central hydrographic station of the outer (T1), middle (T2), and inner (T3) transects. Sampling events are indicated by black triangles. DOI: https://doi.org/10.1525/elementa.438.f4

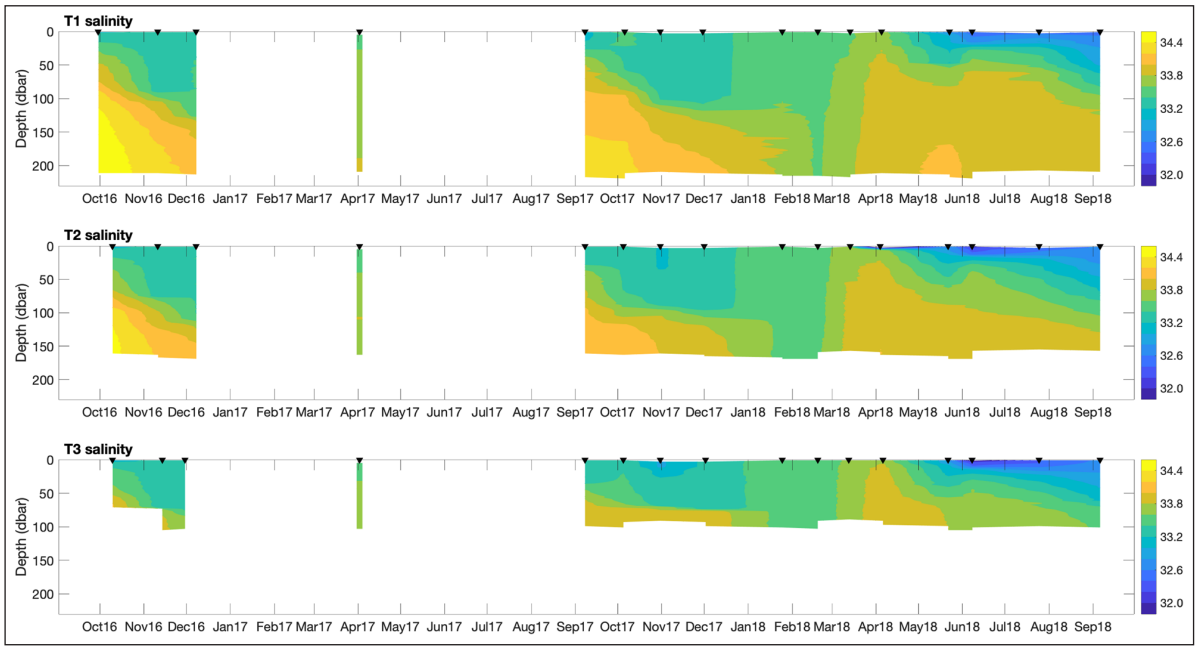

Figure 5: Time series of seawater salinity from October 2016 to September 2018. Measurements of seawater salinity (color scale bar) from CTD deployments at the central hydrographic station of the outer (T1), middle (T2), and inner (T3) transects. Sampling events are indicated by black triangles. DOI: https://doi.org/10.1525/elementa.438.f5

(below 200 m depth) had mean *S* of 34.17 ± 0.24 and θ of 5.35 ± 1.64°C (n = 16). Lowest salinity surface water (*S* of 31.85), thus highest freshwater fraction (**Figure 7a,i,q**), was found in summer in the inner fjord. Temperature maxima occurred in the surface layer in July 2018. The stable oxygen isotope ($\delta^{18}O$) varied between –0.26‰ and 0.76‰ in the water column (**Figure 7b,j,r**). Lower (isotopically depleted) $\delta^{18}O$ is a signal of meteoric water input and was found in the fresher, stratified surface layer from May to November. Higher $\delta^{18}O$ (isotopically enriched) values are indicative of coastal water (with $\delta^{18}O$ 0.44 ± 0.21‰) in the full water column from December until April.

Macronutrients

Water column concentrations of nitrate (NO_3), phosphate (PO_4) and silicic acid ($Si(OH)_4$) had ranges of 0–10.69 µmol kg^{-1}, 0–0.97 µmol kg^{-1} and 0–12.53 µmol kg^{-1}, respectively (**Figure 7**). Lowest concentrations and

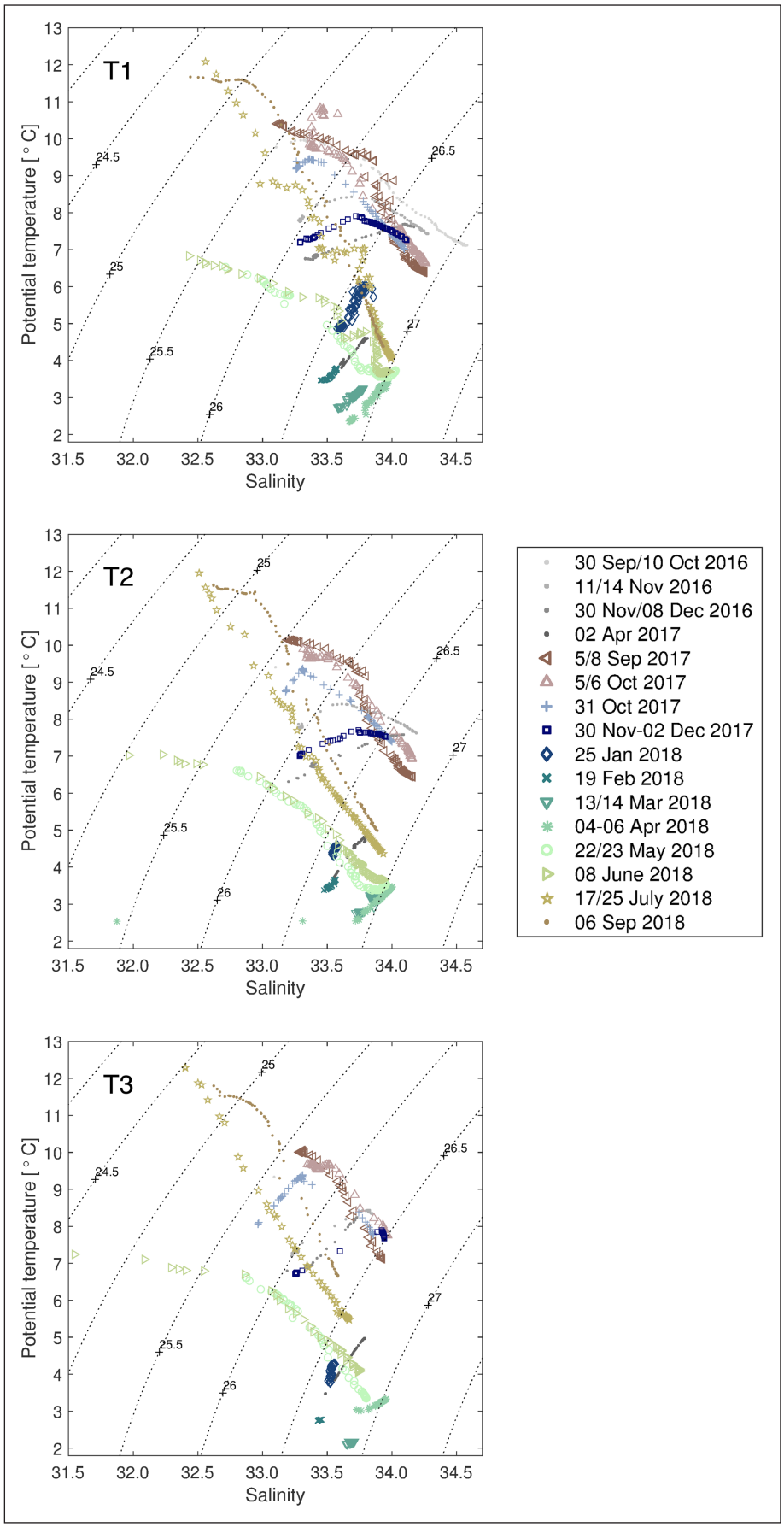

Figure 6: Potential temperature-salinity plots from October 2016 to September 2018. Potential temperature (θ, °C) and salinity characteristics, overlying contours of potential density (kg m^{-3}) anomaly, for all CTD casts at the central hydrographic station of the outer (T1), middle (T2), and inner (T3) transects per sampling event. DOI: https://doi.org/10.1525/elementa.438.f6

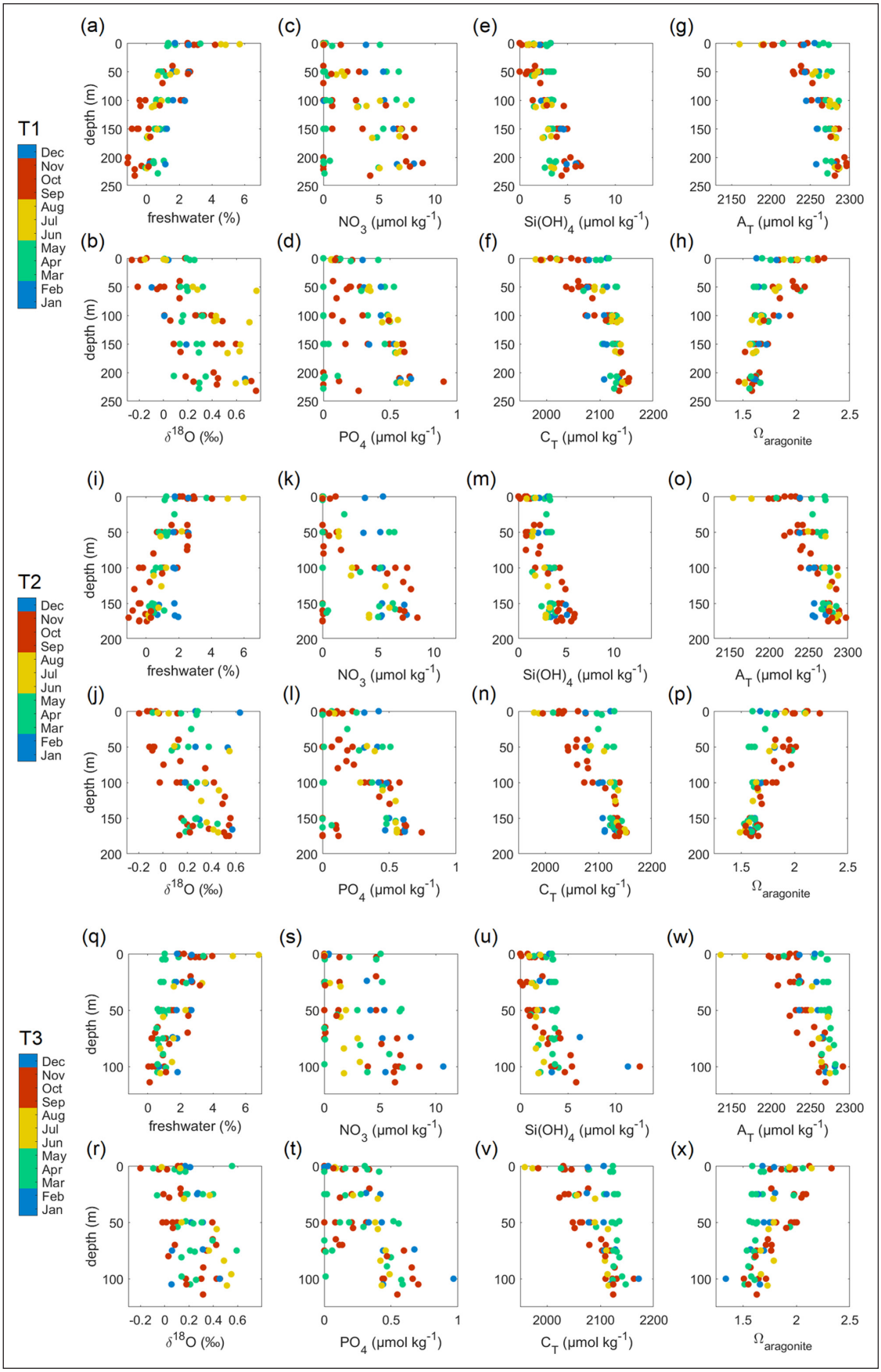

Figure 7: Hydrographic and biogeochemical depth profiles. Depth profiles in the full water column of **(a,i,q)** freshwater fraction (%), **(b,j,r)** $\delta^{18}O$ (‰), **(c,k,s)** nitrate (NO_3, µmol kg^{-1}), **(d,l,t)** phosphate (PO_4, µmol kg^{-1}), **(e,m,u)** silicic acid ($Si(OH)_4$, µmol kg^{-1}), **(f,n,v)** C_T (µmol kg^{-1}), **(g,o,w)** A_T (µmol kg^{-1}), **(h,p,x)** aragonite saturation state (Ω) per sampling month (color bar) at the central hydrographic station of the outer (T1), middle (T2), and inner (T3) transects. DOI: https://doi.org/10.1525/elementa.438.f7

episodic depletion of all macronutrients occurred in the surface layer between June and October across the fjord. Concentrations typically increased with depth but were spatially variable; enriched NO_3 and $Si(OH)_4$ was found at 100-m depth in the inner fjord in December (**Figure 7s,u**). The modified Norwegian Coastal Water (below 200-m depth at T1) had average (n = 16) concentrations of NO_3, PO_4 and $Si(OH)_4$ of 3.79 ± 3.55 µmol kg^{-1}, 0.35 ± 0.31 µmol kg^{-1} and 4.49 ± 1.19 µmol kg^{-1}, respectively, that resupplied the upper layers during vertical mixing.

Carbonate chemistry

The distribution of C_T and A_T showed lower values in the upper 50 m from June to November across the fjord. Surface water C_T was lowest (<2050 µmol kg^{-1}) in summer (**Figure 7f,n,v**) and autumn, and A_T was lowest (<2210 µmol kg^{-1}) from spring to autumn (**Figure 7g,o,w**). Reductions in sea surface C_T and A_T occurred from April, reaching lowest values of 1958 µmol kg^{-1} and 2136 µmol kg^{-1}, respectively, in June 2018. Concentrations of C_T increased with depth to >2105 µmol kg^{-1} below 100 m. The modified Norwegian Coastal Water (below 200 m depth at T1) was characterised by high A_T and C_T of 2257–2296 µmol kg^{-1} and 2108–2154 µmol kg^{-1}, respectively, throughout the study period. Highest C_T of ~2170 µmol kg^{-1} was found close to the seafloor in November in the inner fjord. Aragonite saturation (Ω) was highest (2.20–2.33) in the upper 50 m from June to November across the fjord (**Figure 7h,p,x**). Values decreased with depth to low Ω of 1.34–1.66 below 150 m and lowest near the seafloor in the inner fjord.

Surface water seasonality and air–sea CO_2 exchange

Surface waters (0–5 m) were relatively warm (9.95–12.27°C) and fresh (<33.10) with isotopically light $\delta^{18}O$ (between –0.1‰ and –0.2‰) from July to October (**Figure 8a–c**). NO_3, PO_4 and $Si(OH)_4$ were rapidly reduced in April, with NO_3 and PO_4 nearly totally depleted from

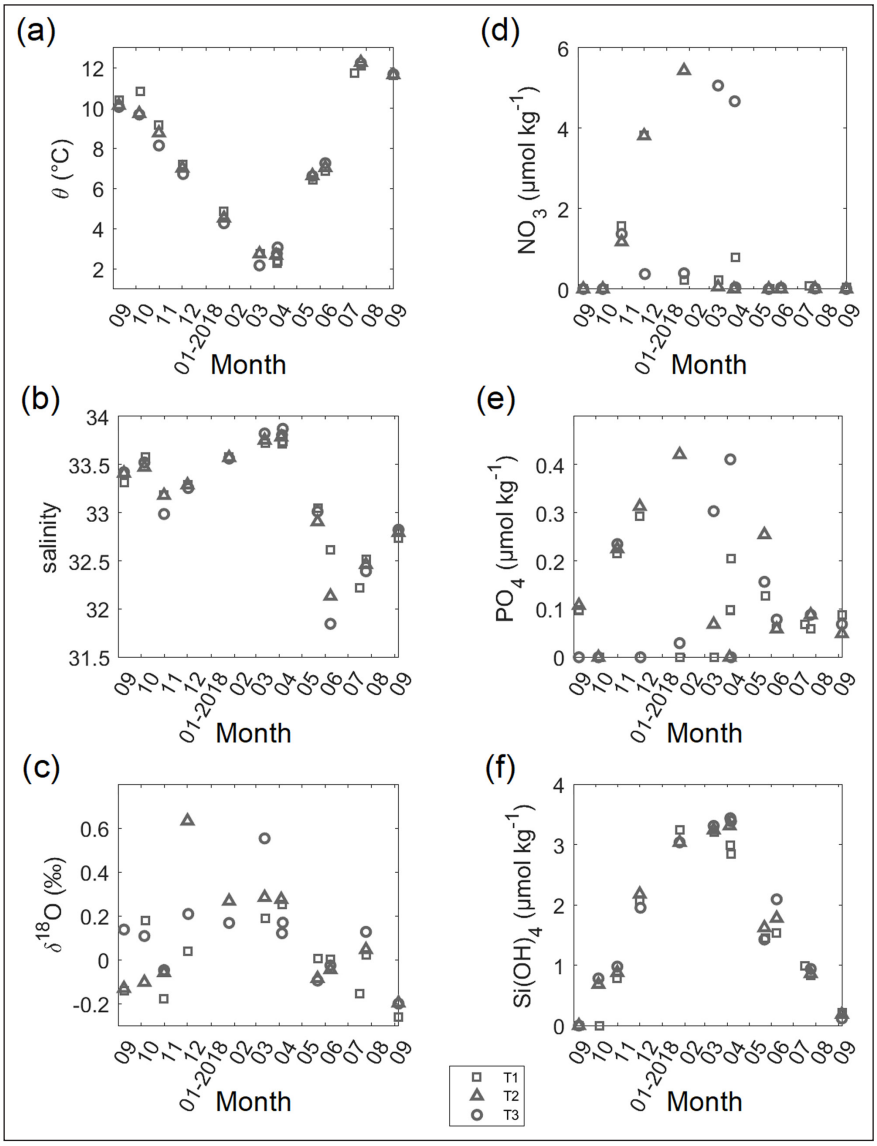

Figure 8: Hydrographic and biogeochemical seasonal cycles in surface water. Surface (0.5 m) water **(a)** potential temperature (°C), **(b)** salinity, **(c)** $\delta^{18}O$ (‰), **(d)** nitrate (NO_3, µmol kg^{-1}), **(e)** phosphate (PO_4, µmol kg^{-1}), **(f)** silicic acid ($Si(OH)_4$, µmol kg^{-1}) per sampling event at the central hydrographic station of the outer (T1), middle (T2), and inner (T3) transects. DOI: https://doi.org/10.1525/elementa.438.f8

May to October (**Figure 8d–f**). Lowest $C_{T\,sal}$ (2059–2065 µmol kg^{-1}), controlled by biological drawdown, and $A_{T\,sal}$ (2250 µmol kg^{-1}), from a likely calcification signal, occurred in September and October (**Figure 9b–c**). Depleted $Si(OH)_4$ also occurred at this time. Surface water fCO_2 was lowest (270–294 µatm) and strongly undersaturated ($\Delta fCO_{2(sea\text{-}air)}$ of –131 µatm) in April and May (**Figure 9d–e**). Greatest CO_2 uptake (2.7 mmol m^{-2} day^{-1}) occurred when $\Delta fCO_{2(sea\text{-}air)}$ was large (–129 µatm) and monthly wind speeds exceeded the yearly average (3.2 m s^{-1}) in May. Ω increased to highest saturation states (2.26–2.33) in September (**Figure 9f**). Seawater CO_2 is influenced by temperature (+1°C raises fCO_2 by about 10 µatm; Takahashi et al., 1993). For a seasonal surface water increase of 10.1°C, increases in fCO_2 up to 100 µatm could be expected. Surface water fCO_2 was found to increase by ~60 µatm, thus the thermodynamic effects were compensated by photosynthetic CO_2 uptake. When the effects of temperature were removed, variations in $fCO_{2\,T}$ showed similar changes compared with fCO_2 (**Figure 9d**) but with a larger seasonal amplitude, suggesting that biological processes dominated over thermodynamic control of fCO_2 to drive strong seasonality in surface water fCO_2 across the fjord (**Figure 10**).

The lowest salinity and highest freshwater fractions (5–6%) in June 2018 were accompanied by increases in $Si(OH)_{4\,sal}$ (~0.8 µmol kg^{-1}) and $C_{T\,sal}$ (~25 µmol kg^{-1}), indicating terrestrial sources of (remineralised) organic matter and weathered minerals entered the fjord during intense precipitation and runoff events. Cold (2.17–3.76°C) and saline (33.58–33.87) surface waters in March and April had enriched $\delta^{18}O$ due to vertical mixing with subsurface

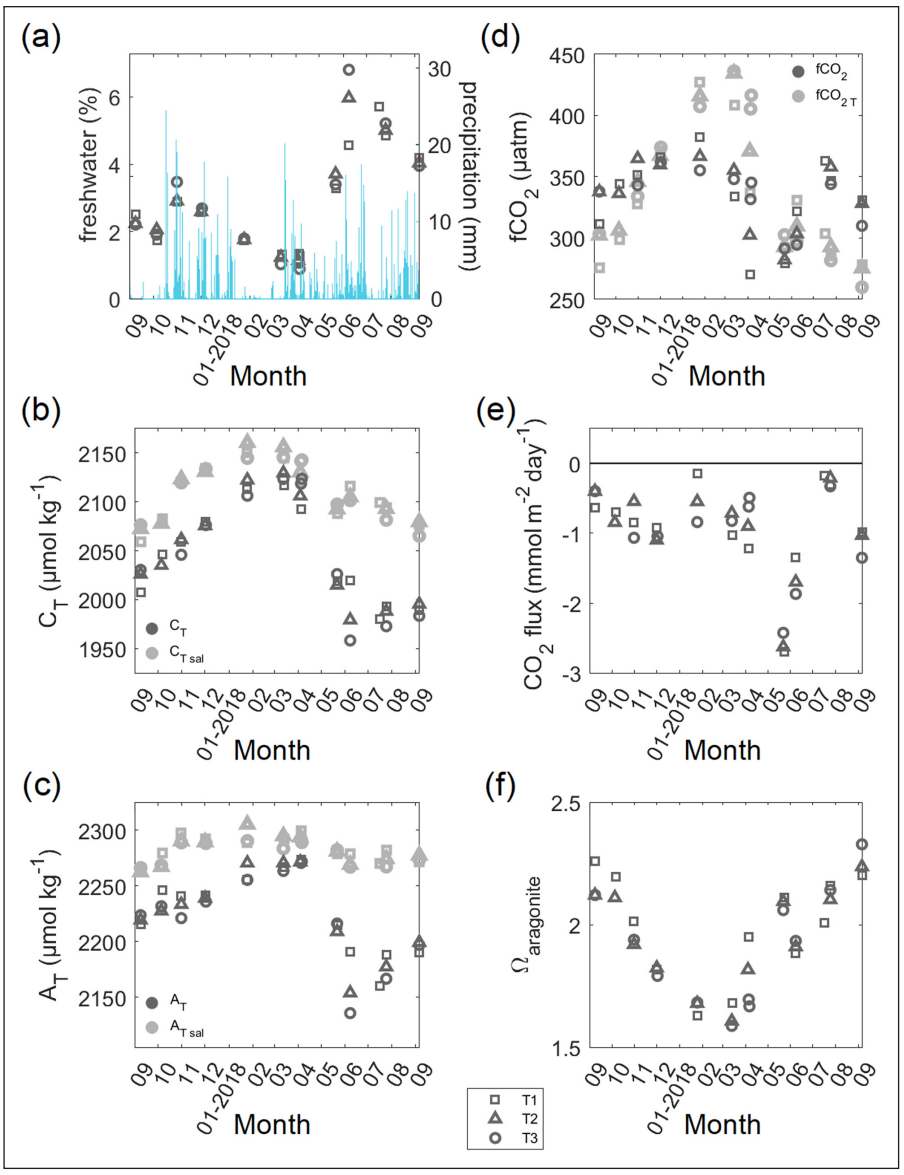

Figure 9: Hydrographic, meteorological and biogeochemical seasonal cycles in surface water. Surface (0–5 m) water **(a)** freshwater fraction (%) and precipitation per 24 hours (mm day^{-1}), **(b)** C_T (µmol kg^{-1}), **(c)** A_T (µmol kg^{-1}), **(d)** fCO_2 (µatm), **(e)** air–sea CO_2 flux (mmol m^{-2} day^{-1}), **(f)** aragonite saturation state (Ω) per sampling event at the central hydrographic station of the outer (T1), middle (T2), and inner (T3) transects. Salinity-normalised C_T and A_T ($C_{T\,sal}$, $A_{T\,sal}$) and temperature-normalised fCO_2 ($fCO_{2\,T}$; fCO_2 measured at in situ temperature normalised to average temperature of all data) are shown in their respective plots in grey. DOI: https://doi.org/10.1525/elementa.438.f9

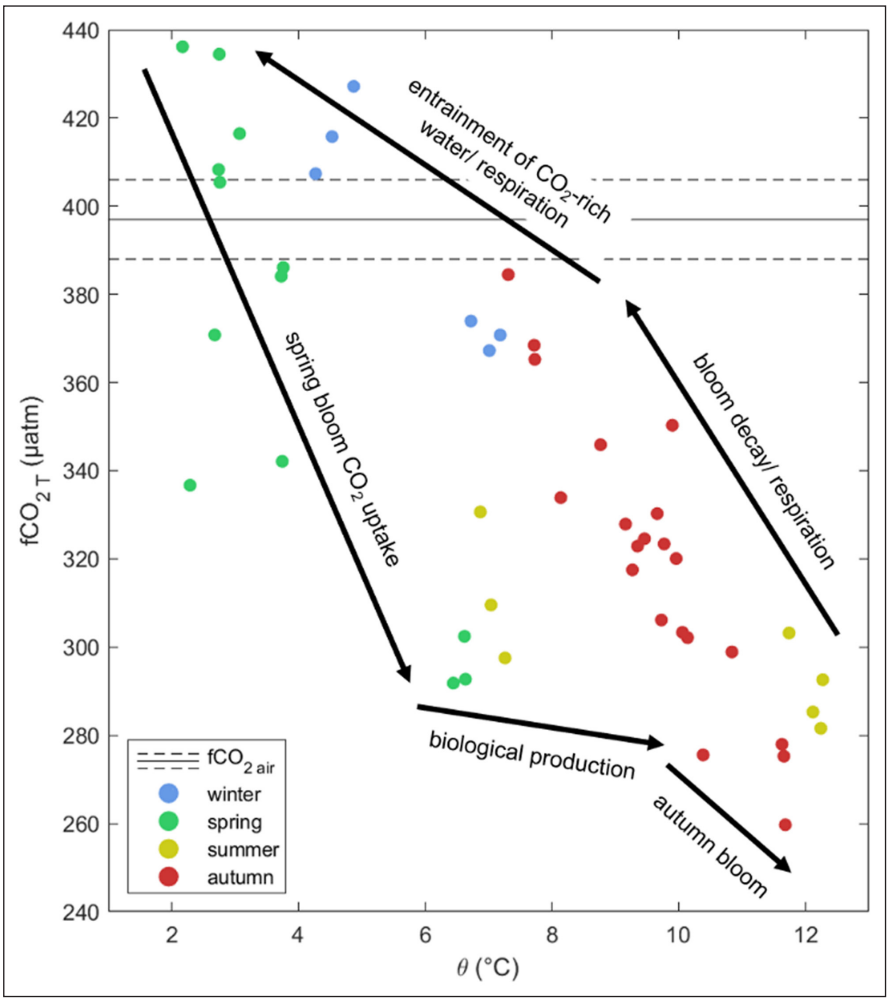

Figure 10: Seasonality in fCO_2 driven by biological processes. Surface water temperature-normalised fCO_2 ($fCO_{2\,T}$, µatm) as a function of potential temperature (θ, °C) per season (by color) with key biological processes marked. The fCO_2 in air ($fCO_{2\,air}$, µatm) average (solid black line) and standard deviation (dashed lines) during the 2017–2018 annual cycle is indicated. The fCO_2 data below the $fCO_{2\,air}$ lines indicate undersaturation with respect to the atmosphere and increased potential for CO_2 uptake. DOI: https://doi.org/10.1525/elementa.438.f10

coastal water. Respiration, remineralisation and vertical mixing of the water column increased $C_{T\,sal}$, $NO_{3\,sal}$, $PO_{4\,sal}$ and $Si(OH)_{4\,sal}$, with a potential contributions from silicate dissolution, from January to March. The maximum absolute difference between measured and salinity-normalised concentrations for NO_3, PO_4 and $Si(OH)_{4\,sal}$ was 0.13 µmol kg^{-1}, 0.01 µmol kg^{-1} and 0.15 µmol kg^{-1}, respectively, and relatively minor compared to 143 µmol kg^{-1} for C_T and 131 µmol kg^{-1} for A_T. Increases in $A_{T\,sal}$ by ~40 µmol kg^{-1} occurred from early autumn to November. Surface water Ω was less variable during winter/early spring and lowest values (1.59) in March. fCO_2 was highest (381–388 µatm) between September and February, and $fCO_{2\,T}$ peaked in January–March, which coincided with the period of convective mixing and colder temperatures. Surface waters were undersaturated with respect to atmospheric CO_2 with an average $\Delta fCO_{2(sea\text{-}air)}$ of –58 ± 33 µatm (n = 46), driving air–sea CO_2 exchange of –0.86 ± 0.63 mmol m^{-2} day^{-1} (n = 46; atmospheric CO_2 uptake). On an annual basis, the surface layer in Kaldfjorden is estimated to be a sink for atmospheric CO_2 of 0.32 ± 0.03 mol C m^{-2} yr^{-1} (n = 12).

Seasonal mixed layer carbonate chemistry dynamics

The largest total monthly change in C_T ($\Delta C_{T\,total}$) in the upper 50 m was –4.1 mol m^{-2} $month^{-1}$, in the inner fjord, driven by changes in salinity $\Delta C_{T\,sal}$ of –3.3 mol m^{-2} $month^{-1}$ (accounting for 81% of $\Delta C_{T\,total}$) due to freshwater inputs in June (**Figure 11**). $\Delta C_{T\,mix}$ showed little variation in its range of 0–0.1 mol m^{-2} $month^{-1}$, constituting up to 5% of $\Delta C_{T\,total}$. The upper percentages of $\Delta C_{T\,mix}$ contributions coincided with the timing of erosion of water column stratification and increased C_T in the upper layers from mixing with subsurface Norwegian Coastal Water, notably from December to April. $\Delta C_{T\,bio}$ ($\Delta C_{T\,bio\,C}$; determined from the residual difference between $\Delta C_{T\,total}$ and all other factors) ranged between –0.4 mol m^{-2} $month^{-1}$ and –0.8 mol m^{-2} $month^{-1}$ during the spring bloom and summer productive period from April to June. Biological production accounted for 20–30% of $\Delta C_{T\,total}$ and coincided with maximum $\Delta C_{T\,bio\,N}$ of –1.2 mol m^{-1} $month^{-1}$ from the rapid NO_3 drawdown in April. A second peak in biological C_T drawdown occurred in August with $\Delta C_{T\,bio\,C}$ up to –0.5 mol m^{-2} $month^{-1}$ as a signal of late summer production and a possible autumn bloom. Greatest increases in $\Delta C_{T\,total}$ of

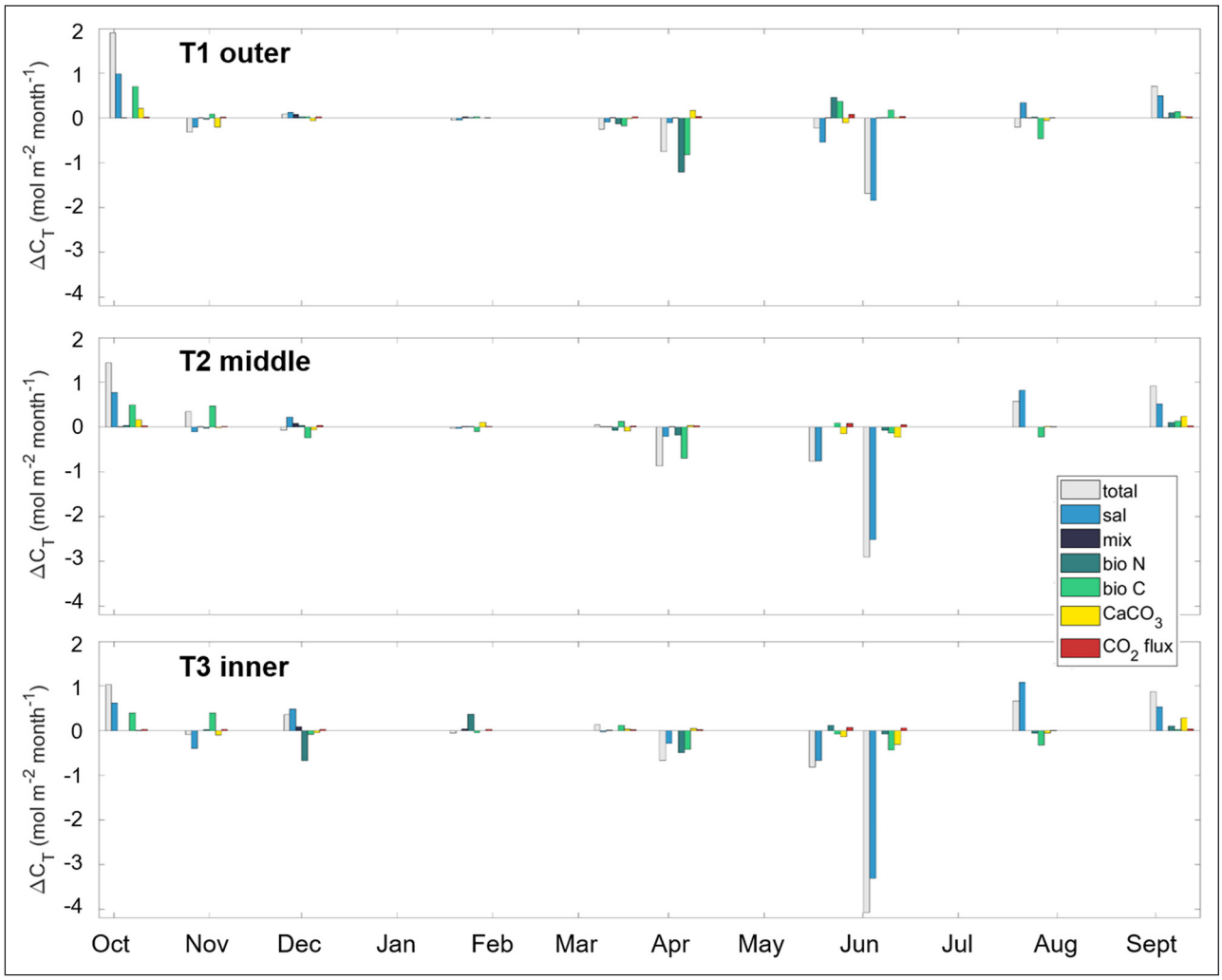

Figure 11: Temporal evolution of C_T in the upper layer during the 2017–2018 annual cycle. Monthly changes in total dissolved inorganic carbon (ΔC_T, mol m^{-2} month^{-1}) in the upper layer (0–50 m) of Kaldfjorden are determined from contributions from salinity changes ($\Delta C_{T\,sal}$), mixing ($\Delta C_{T\,mix}$), photosynthesis/respiration ($\Delta C_{T\,bio}$), calcium carbonate formation/dissolution ($\Delta C_{T\,CaCO_3}$) and air–sea CO_2 exchange ($\Delta C_{T\,flux}$) per sampling month during the 2017–2018 annual cycle at the central hydrographic station of the outer (T1), middle (T2), and inner (T3) transects. $\Delta C_{T\,bio}$ was estimated by (1) using monthly changes in salinity-normalised nitrate and the C/N Redfield ratio of 6.6 (Redfield et al., 1963) to estimate C_T uptake ($\Delta C_{T\,bio\,N}$) and by (2) residual difference between the total C_T change and the sum of all other contributing factors ($\Delta C_{T\,bio\,C}$). DOI: https://doi.org/10.1525/elementa.438.f11

1.4–1.9 mol m^{-1} month^{-1} were driven by $\Delta C_{T\,sal}$ of 1.1 mol m^{-2} month^{-1} (57% of $\Delta C_{T\,total}$) and $\Delta C_{T\,bio\,C}$ of 0.4–0.7 mol m^{-2} month^{-1} (37% of $\Delta C_{T\,total}$) from September to October. These increases were a result of reduction in freshwater fluxes and increased surface layer C_T from respiration and remineralisation (as indicated by higher nutrient concentrations) in post-bloom conditions. $\Delta C_{T\,CaCO_3}(\frac{1}{2}[\Delta A_{T\,CaCO_3}])$ was lowest at –0.3 mol m^{-2} month^{-1}, which accounted for up to 8% of the reduction in $\Delta C_{T\,total}$ due to the presence of calcifying phytoplankton. Highest $\Delta C_{T\,CaCO_3}$ of 0.3 mol m^{-2} month^{-1} represented up to 15% of $\Delta C_{T\,total}$ at the time of intense freshwater runoff, indicating terrestrial inputs of A_T, and a decaying coccolithophore bloom in September. Excess A_T (positive $\Delta C_{T\,CaCO_3}$) could also result from particulate inorganic carbon, e.g., $CaCO_3$ shells in the water column that are captured by sampling and dissolve upon analysis. $\Delta C_{T\,flux}$ range was 0–0.1 mol m^{-2} month^{-1} from the increased C_T in the upper layers due to uptake of atmospheric CO_2, which was highest in May and June (up to 4% of $\Delta C_{T\,total}$).

Monthly change in Ω for aragonite ($\Delta\Omega_{total}$) ranged between –0.43 and 0.37 across Kaldfjorden (**Figure 12**). Greatest increases in ΔΩ were driven by biological production (decreased C_T, slight increase in A_T) as $\Delta\Omega_{bio\,C}$ (and $\Delta\Omega_{bio\,N}$) varied between 0.25 and 0.40 from April to June. Biological production dominated the other processes and accounted for up to 99% of the monthly change in Ω. Increases in $\Delta\Omega_{bio\,C}$ up to 0.20 in August and September coincide with biological C_T drawdown in a late summer/autumn bloom. Respiration (increased C_T, slight decrease in A_T) in post bloom and winter conditions dominated the monthly decreases in $\Delta\Omega_{total}$ with $\Delta\Omega_{bio\,C}$ of –0.50. Lowest (negative) $\Delta C_{T\,CaCO_3}$ corresponded to lowest (negative) $\Delta\Omega_{CaCO_3}$ of –0.09, and 21% of $\Delta\Omega_{total}$, as a result of calcification (greater decreases in A_T relative to C_T) in spring and summer. Lowest (negative) monthly

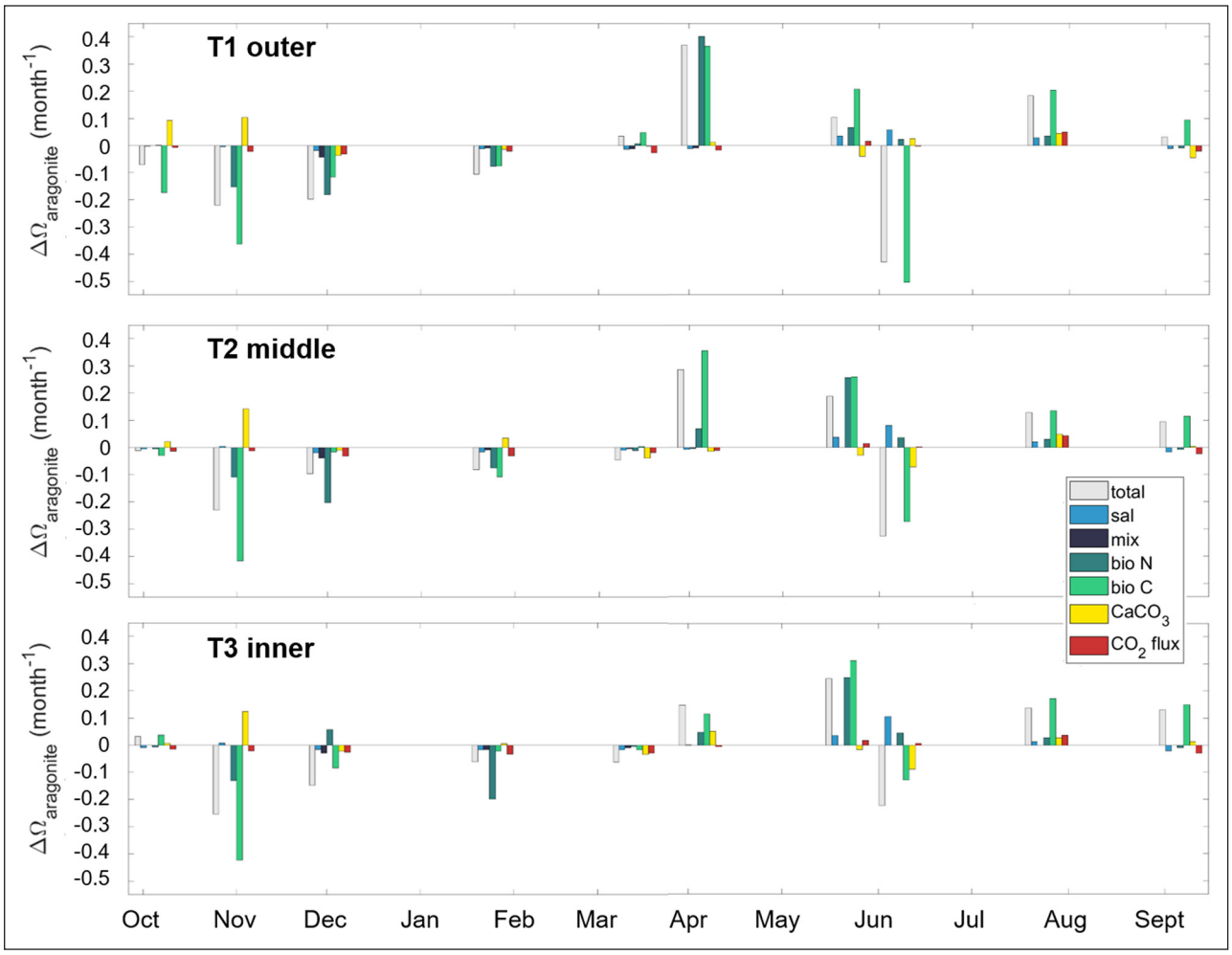

Figure 12: Temporal evolution of surface water Ω during the 2017-2018 annual cycle. Monthly changes in the aragonite saturation state ($\Delta\Omega_{total}$) are determined from monthly changes in ΔC_T and ΔA_T for each of the key physical and biogeochemical processes, salinity changes ($\Delta\Omega_{sal}$), mixing ($\Delta\Omega_{mix}$), photosynthesis/respiration ($\Delta\Omega_{bio}$), calcium carbonate formation/dissolution ($\Delta\Omega_{CaCO_3}$), air–sea CO_2 exchange ($\Delta\Omega_{flux}$) and per sampling month during the 2017–2018 annual cycle at the central hydrographic station of the outer (T1), middle (T2), and inner (T3) transects. DOI: https://doi.org/10.1525/elementa.438.f12

changes in $\Delta C_{T\,sal}$ corresponded to highest (positive) $\Delta\Omega_{sal}$ up to 0.11 to reveal the net effect of C_T dilution offset the effect of decreases in A_T from freshwater inputs. Minor changes in ΔΩ resulted from mixing with subsurface Norwegian Coastal Water, which was largest in winter and early spring with $\Delta\Omega_{mix}$ of –0.04 (representing up to 10% of $\Delta\Omega_{total}$ in December). $\Delta\Omega_{flux}$ ranged between –0.03 in December and January and 0.05 in August from changes in monthly CO_2 uptake and subsequent increased C_T in the surface layer.

Discussion

Seasonality in freshwater and deep-water effects

Higher freshwater fractions (4–7%) and a shift towards depleted $\delta^{18}O$ (–0.26‰) from June to September coincided with warmer air temperatures and higher precipitation. The effects of increased precipitation and river runoff dominated the greatest monthly change in C_T of –4.1 mol C m^{-2}, representing reductions of C_T from dilution effects that accounted for 81% of monthly C_T deficits in the inner part of the fjord in June. Summertime values of C_T and A_T in the surface layer of Kaldfjorden were similar to those reported for Svalbard fjords (Fransson et al., 2015; Ericson et al., 2019b) but generally higher than those of other high-latitude coastal and fjord systems (**Table 2**). The differences are largely due to greater meteoric water inputs in the other high-latitude regions compared to Kaldfjorden, which include glacial meltwater and contributions from sea-ice melt that result in higher dilution effects that lower A_T (and C_T). In combination with strong biological carbon uptake, the fjord and coastal regions at higher latitudes and inland seas have nominally lower surface water A_T and C_T compared to Kaldfjorden.

The importance of freshwater in controlling the carbonate system and nutrient dynamics in Kaldfjorden is evident from the relationship between salinity and A_T and C_T during a full annual cycle (**Figure 13a**). The strong correlation between A_T and salinity yielded $A_T = 56.9S + 337$ ($r^2 = 0.84$, se = 55 µmol kg^{-1}, $p < 0.0001$, $n = 234$), which shows evidence of a freshwater (zero salinity) end-member for A_T of 337 ± 55 µmol kg^{-1}. For C_T and salinity, the relationship yielded $C_T = 82.9S - 696$ ($r^2 = 0.76$;

Table 2: Summer C_T and A_T in surface waters of northern high-latitude coastal and fjord systems and inland seas. DOI: https://doi.org/10.1525/elementa.438.t2

Region	C_T range (µmol kg^{-1})	A_T range (µmol kg^{-1})	Reference
Baltic Sea	1200–2100	–[a]	Thomas and Schneider (1999)
Glacier Bay, Alaska	1273–2044	1412–2137	Reisdorph and Mathis (2014)
Puget Sound, Pacific Northwest, USA	1431–2038	1510–2101	Pelletier et al. (2018)
Cumberland Sound, Canadian Arctic	1779–1978	1922–2147	Turk et al. (2016)
Tempelfjorden, Svalbard	1960–2080	2130–2260	Fransson et al. (2015)
Adventfjorden, Svalbard	2050–2060	2060–2150	Ericson et al. (2019b)
Kaldfjorden, northern Norway	1958–2129	2136–2273	this study

[a] Not available.

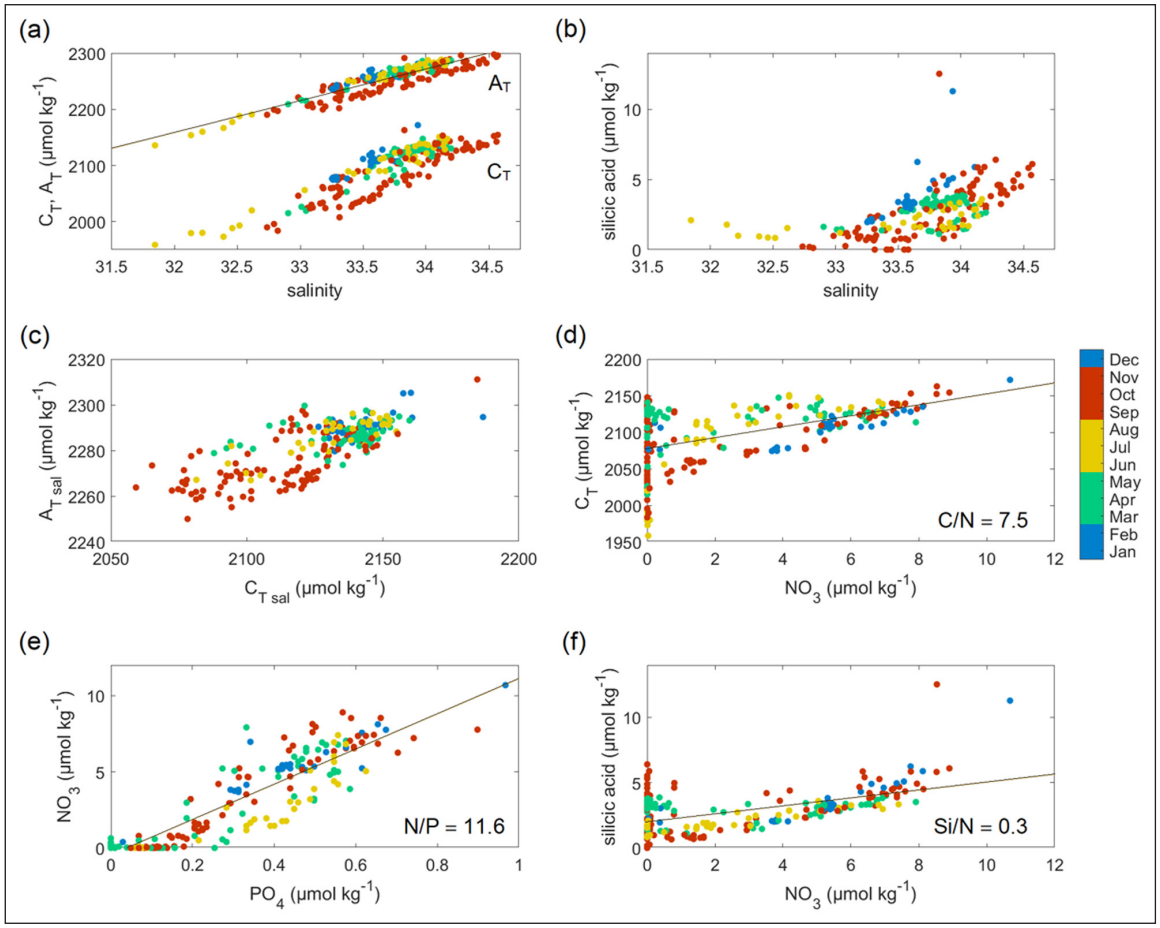

Figure 13: Key carbonate chemistry, nutrients and salinity seasonal cycles and relationships. Trends in water column **(a)** C_T (µmol kg^{-1}), A_T (µmol kg^{-1}) and salinity, **(b)** silicic acid ($Si(OH)_4$, µmol kg^{-1}) and salinity, **(c)** $C_{T\,sal}$ (µmol kg^{-1}) and $A_{T\,sal}$ (µmol kg^{-1}), **(d)** C_T (µmol kg^{-1}) and nitrate (NO_3, µmol kg^{-1}), **(e)** nitrate (NO_3, µmol kg^{-1}) and phosphate (PO_4, µmol kg^{-1}), **(f)** silicic acid ($Si(OH)_4$, µmol kg^{-1}) and nitrate (NO_3, µmol kg^{-1}) per sampling month (color bar) at the central hydrographic station of the outer (T1), middle (T2), and inner (T3) transects. Carbon and nutrient uptake/regeneration ratios (C/N, N/P, Si/N) determined from the linear regression trend of all seasonal data are shown in their respective plots. DOI: https://doi.org/10.1525/elementa.438.f13

se = 102 µmol kg^{-1}; $p < 0.0001$: $n = 235$), which indicates a deficit in C_T in freshwater, as reported for freshwater A_T endmember estimates from salinity relationships by Turk et al. (2016). A second approach in estimating the freshwater A_T endmember is using the relationship with $\delta^{18}O$, as a comparison. Firstly, the meteoric $\delta^{18}O$ signature of freshwater was estimated as –10.1‰ from the relationship between $\delta^{18}O$ and salinity ($r^2 = 0.43$, se = 0.79‰, $p < 0.0001$, $n = 226$). As no direct measurements of freshwater endmembers are currently available for Kaldfjorden,

the $\delta^{18}O$ (–10.1‰) value determined here indicates that the freshwater sources are predominantly of meteoric origin (snow melt, precipitation and river runoff). The estimated $\delta^{18}O$ value in Kaldfjorden is similar to that of the Hudson Bay rivers (latitude ~60°N) and falls at the higher end (isotopically heavier) of previously reported ranges of $\delta^{18}O$ in meteoric water endmembers in other high latitude fjord and coastal systems (**Table 3**). The spatial variability of the freshwater $\delta^{18}O$ signature is due to the fact that precipitation becomes increasingly light isotopically at higher latitudes, in addition to localised variations such as influences of glaciers in sub-Arctic regions, as suggested by Turk et al. (2016).

When applied to the A_T-$\delta^{18}O$ linear regression $A_T = 88.7\delta^{18}O + 2236$ ($r^2 = 0.44$, se = 6.7 μmol kg^{-1} ‰$^{-1}$, $p < 0.0001$, $n = 223$), the A_T endmember is estimated at 1340 ± 9 μmol kg^{-1}. The range of the estimated freshwater A_T endmember (337–1340 μmol kg^{-1}) for Kaldfjorden falls within the range of Arctic rivers (Cooper et al., 2008) and for the Svalbard fjords (Fransson et al., 2015; Ericson et al., 2019a, 2019b), which are influenced by glacial runoff with a watershed containing carbonate and silicate bedrock. Values were higher than those for meteoric endmembers dominated by glacial meltwater in Greenland (Meire et al., 2015) and for Cumberland Sound (Turk et al., 2016). The associated freshwater source of A_T likely originates from terrestrial inputs, e.g., weathered minerals of surrounding rock. The regression analysis showed that freshwater in Kaldfjorden had a diluting impact on surface water A_T. The freshwater-derived A_T would act to slightly decrease dilution effects; however, the overall effect from freshwater inputs is a lowering of A_T (and C_T) in the surface layer. Variations in the A_T content of meteoric water have been previously attributed to river drainage over carbonate and silicate-rich rocks that subsequently become enriched with minerals and transported into the fjord and coastal waters (Hjalmarsson et al., 2008; Azetsu-Scott et al., 2014; Fransson et al., 2015; Ericson et al., 2019a).

Similarly to A_T, C_T decreased with increasing freshwater inputs in the upper layer of the fjord. From linear regression analysis with the local $\delta^{18}O$ endmember (–10.1‰), $A_T = 140.1\delta^{18}O + 2066$ ($r^2 = 0.47$, se = 9.9 μmol kg^{-1} ‰$^{-1}$, $p < 0.0001$, $n = 224$), the freshwater C_T endmember was estimated as 651 ± 13 μmol kg^{-1}. In contrast to the endmember estimates for A_T, the C_T estimates are similar in magnitude but opposite in sign. These findings suggest that the freshwater salinity and $\delta^{18}O$ system could be influenced by contrasting processes of inorganic carbon removal and enrichment, respectively, depending upon which estimation method was selected. The $\delta^{18}O$-based endmember is similar to the estimated C_T endmember in Tempelfjorden, Svalbard (Ericson et al., 2019a). This similarity leads to the hypothesis that freshwater runoff could contain a source of C_T derived from atmospheric CO_2 uptake and terrestrial organic matter, which was subsequently remineralised upon transport to and release into the fjord. Increased surface water $Si(OH)_4$ and $C_{T\,sal}$ of ~25 μmol kg^{-1} that was linked to persistent precipitation, most notably at the inner part of the fjord, indicated a supply of dissolved silica, perhaps from weathered silicate minerals, within freshwater runoff (**Figure 13b**). The enhanced surface water $C_{T\,sal}$ associated with freshwater fluxes enriched the C_T pool of the fjord and led to reductions in Ω. However, any additional C_T was likely assimilated during biological production during the summer and thus constitutes a more transient signal following prolonged precipitation as observed in June 2018. Enhanced A_T and silicates in freshwater delivered to Kaldfjorden could

Table 3: Literature values, ranges or mean ± standard deviation (n value) of measured and estimated $\delta^{18}O$, C_T and A_T in meteoric water endmembers in northern high-latitude fjord and coastal systems. DOI: https://doi.org/10.1525/elementa.438.t3

Region	$\delta^{18}O$ (‰)	C_T (μmol kg^{-1})	A_T (μmol kg^{-1})	Reference
Godthåbsfjord, west Greenland	na[a]	80 ± 17	50 ± 20	Meire et al. (2015)
Siberian rivers; North American Arctic rivers	–20.5, –14.9	na	800–1900	Cooper et al. (2008)
Cumberland Sound, Canadian Arctic	–19.2 ± 0.8 (40)	247	174	Turk et al. (2016)
Hudson Bay rivers, Canada	–16.8, –10.8	na	226–1870	Burt et al. (2016)
Adventfjorden, Svalbard	na	339 ± 7[b]	294 ± 3[b], 418	Ericson et al. (2018, 2019b)
Tempelfjorden, Svalbard	–16, –4.9	508 ± 52 (n = 36), 661 ± 45 (n = 27)	526–1142; 355 ± 24 (n = 36), 601 ± 42 (n = 27)	Fransson et al. (2015); Ericson et al. (2019a)
Kongsfjorden, Svalbard	–15.9	na	890	Maclachlan et al. (2007); Fransson et al. (2016)
Kaldfjorden, northern Norway	–10.1 ± 0.8 (n = 226)	651 ± 13 (n = 224)	337 ± 55 (n = 234), 1340 ± 9 (n = 223)	this study

[a] Not available in the cited reference.
[b] N value not stated in the cited reference.

constitute a minor buffer in the surface layer against CO_2 increases and provide an additional source of silicate to siliceous plankton species, e.g., diatoms. Future warming and increased precipitation and runoff in the sub-Arctic will result in higher freshwater inputs but, in regions of calcareous and siliceous bedrock, a terrestrial supply of dissolved minerals could act to slightly counteract dilution effects on seawater A_T.

The seasonality in A_T and C_T in the modified Norwegian Coastal Water below 200 m at the mouth of the fjord varied from lower values in winter and higher values in summer and autumn as evidence of convective mixing of the surface layer and subsurface coastal water when stratification becomes eroded (**Figure 7f–g**). Deep vertical mixing in winter and spring, as indicated by a shift in $\delta^{18}O$ from higher (~0.6‰) to lower (~0.1‰) isotopic values, homogenised the water column and enabled the coastal water source of macronutrients to be entrained into the upper layers and the freshwater-influenced surface to permeate deeper (**Figure 7a–b**). As such, the A_T and C_T signal from the productive surface layers was dispersed into the water column and lowered A_T and C_T. Following spring and summer biological production, enriched C_T and macronutrients were found at 150–250 m depth, with highest concentrations in November and December. This is due to enrichment from organic matter sinking out of productive surface waters and being remineralised in the subsurface and deep water. Seasonal variability in deep water A_T and $Si(OH)_4$ closely followed variations in salinity and $\delta^{18}O$. Higher A_T in November and December likely includes a contribution from sediment resuspension, superimposed onto the relatively elevated A_T signal from Norwegian Coastal Water (with $\delta^{18}O$ of ~0.8). Increased concentrations of $Si(OH)_4$ arise from remineralisation of silicates, e.g., from diatoms and sediment resuspension, during wind-induced mixing.

The impact of these competing processes that increase and decrease C_T and A_T, largely removed net seasonality from Ω variations below 150 m, yielding a narrow range of Ω (1.5–1.7) throughout the year. A notable increase in concentrations of all macronutrients and C_T was found close to the sea floor at the inner part of the fjord in December 2017, which resulted in the lowest Ω of 1.3 during the time series. This low Ω could result from remineralisation, sediment fluxes or perhaps a manmade signal, for example water discharge in the shallower part of the fjord closest to land. This signal appeared to be localised and showed impacts to carbonate chemistry in areas exposed to greater land-water interactions, i.e., higher C_T inputs reduced Ω. Removing the effects of salinity changes on C_T and A_T (**Figure 13c**) reveals further seasonal dynamics driven by biological production, calcification and atmospheric CO_2 uptake (discussed in the following section).

Seasonal biological processes and NCP

The importance of biological processes on the carbonate chemistry in Kaldfjorden is reflected in the seasonal NCP and substantial C_T drawdown during spring and summer (**Figure 11**). With greater light availability, phytoplankton biomass increased in early spring and developed into a bloom of diatoms and *Phaeocystis* with chlorophyll *a* concentrations up to 10 mg m^{-3} in April (Persson, 2018). Weak stratification and nutrient replenishment from subsurface waters and recycling in the upper water column fuelled biological production. Peaks in particulate matter fluxes and chlorophyll *a* fluxes, out of the surface layer during the spring bloom, have been observed in a neighbouring fjord, Balsfjorden in Tromsø (Eilertsen et al., 1981; Eilertsen and Degerlund, 2010). Coupled to strong biological carbon uptake and conversion to organic carbon, subsequent export of organic matter would contribute to reductions in water column C_T. Some organic matter may settle out of the water column and become buried in the sediments, driving seasonal ΔC_T depletion in the upper layer of the fjord during April. The abundance of zooplankton, e.g., copepods, was low, and export of particulate organic carbon likely continued prior to the development of strong stratification by late spring that would impede export of particulate matter to depth (Wassmann et al., 1991; Walker, 2018). By June and July, stronger stratification likely inhibited export of organic matter across the pycnocline, and thus respiration and recycling in the upper layers contributed to reduced monthly change in $\Delta C_{T\,bioN}$ and net respiration signals relative to April.

NCP estimates were determined from the residual difference between the total monthly change in depth-integrated C_T and the sum of all other contributing factors ($\Delta C_{T\,bio\,C}$; NCP_C) and from the total monthly change in depth-integrated NO_3, corrected for salinity changes ($\Delta C_{T\,bio\,N}$; NCP_N). During the productive months (growing season) of April–August, NCP_C was 14 ± 2 g C m^{-2} ($n = 5$), which is about twice as large than the NCP_N estimate of 6 ± 2 g C m^{-2} ($n = 5$). The differences in NCP_C and NCP_N for both seasonal and annual estimates arise from the sensitivity of the nitrate-based estimates to the C/N ratio selected. NCP is often computed using the Redfield ratio of C:N:P 106:16:1 (Redfield, 1963), which is most suitable when nitrate and phosphate are not depleted and C_T, NO_3 and PO_4 are assimilated and regenerated following the Redfield proportions (Arrigo, 2005). The relationship between C_T and NO_3 (**Figure 13d**) yielded an average C/N of 7.5 ($r^2 = 0.26$, se = 0.83 μmol kg^{-1}, $p \ll 0.001$, $n = 233$) with a tendency towards lower C/N uptake ratios in the spring as a result of rapid NO_3 consumption as C_T remained high, followed by a shift to higher C/N uptake ratios in the summer and early autumn upon intense drawdown of C_T during high NCP. These C/N uptake ratios are higher than the Redfield C/N ratio (6.6) and consistent with previous observations of Frigstad et al. (2014) of C/N ratios that are higher relative to Redfield stoichiometry in northern high latitude regions, such as 6.7–7.0 in the Norwegian Sea region.

The strong de-coupling of C_T and NO_3 at near-total depletion of NO_3 persisted during the growing season, suggesting that rapid recycling of nutrients, production of nitrogen-poor organic matter and/or other sources of nitrogen, such as ammonia, could be important factors (Kähler and Koeve, 2001). Furthermore, the C/N uptake ratio is likely to vary due to phytoplankton species composition (Sambrotto et al., 1993) and availability of dissolved

iron (Takeda, 1998). As such, carbon-based estimates often exceed nitrogen-based estimates of NCP (Bozec et al. 2006; Tremblay et al. 2008; Ericson et al., 2019b). In addition, changes in light, temperature, salinity and availability of micro-nutrients are all likely to play a role. Therefore, using the traditional Redfield utilisation/replenishment ratio would not constrain the depletion in C_T relative to NO_3 in Kaldfjorden, and N-based NCP estimates would not capture the extent of biological carbon uptake. Lower C/N in the winter and spring coincided with the smallest biologically driven monthly C_T deficits and was dominated by enrichment from respiration and remineralisation. Breakdown in water column stratification, mixing and diminishing light led to a steep decline in chlorophyll *a* concentrations (0.03–0.12 mg m^{-3}) and zooplankton abundance from October to February (Walker, 2018). The closer coupling of C and N at higher concentrations is evidence of export and remineralisation of organic matter in (sub-)surface waters, with likely contributions from sediment resuspension following episodic high winds (Walker, 2018) during winter.

The relationships between NO_3 and PO_4 (N/P; **Figure 13e**) and $Si(OH)_4$ and NO_3 (Si/N; **Figure 13f**) inform about the differences in supply and consumption of macronutrients. The average N/P was 11.6 (r^2 = 0.83, se = 0.34 µmol kg^{-1}, $p \ll 0.001$, n = 240) and shows close coupling of inorganic nitrogen and phosphorus. The N/P values were slightly lower in winter and higher in autumn. The temporal trends in N* (**Figure 14a**) and lower N/P observed during winter and early spring result from the

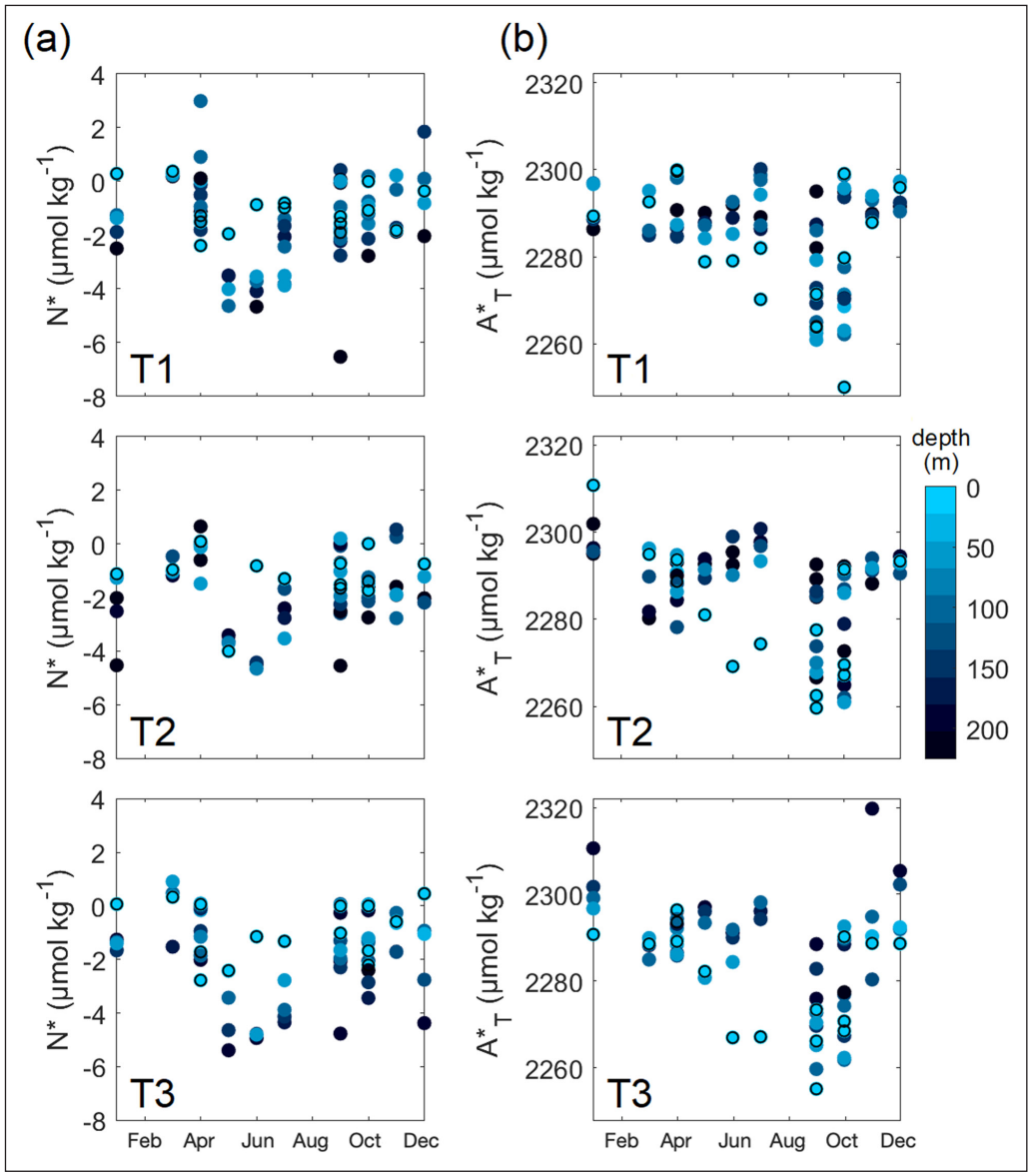

Figure 14: Monthly variability in N* and potential alkalinity. The seasonal cycle of **(a)** N* (µmol kg^{-1}; $[NO_3 + NO_2] - 16[PO_4]$) (Gruber and Sarmiento, 1997); see section *Water sampling and analysis*), **(b)** potential alkalinity (A^*_T, µmol kg^{-1}; the sum of salinity-normalised A_T and NO_3 (Brewer and Goldman, 1976); see section *Carbonate system determinations*) for the full water column per sampling depth (m, color scale bar) for each month at the central hydrographic station of the outer (T1), middle (T2), and inner (T3) transects. Surface (0–5 m) water data are indicated by open black circles. DOI: https://doi.org/10.1525/elementa.438.f14

rapid removal of NO_3, and PO_4, in the spring bloom. NCP increased from April as primary production exceeded respiration and caused a rapid reduction in C_T in the surface layer. Reductions in N* from May show a shift in the system as nitrogen is depleted by ongoing biological production combined with denitrification and/or advective losses and remineralisation in subsurface water of organic matter with lower N/P ratios. The average seasonal Si/N was 0.3 ($r^2 = 0.28$, se = 0.03 μmol kg^{-1}, $p \ll 0.001$, $n = 240$) and shows variability and weak coupling with an excess of $Si(OH)_4$ relative to NO_3 at low NO_3 concentrations. Surface water NO_3 was depleted from May to October, while $Si(OH)_4$and C_T were continually consumed due to biological production by a diatom community. In addition, any iron limitation in the fjord would result in phytoplankton assimilating less NO_3 relative to $Si(OH)_4$, thus contributing to higher Si/N (Takeda, 1998), as observed in autumn.

The time lag in $Si(OH)_4$ drawdown of about one month, accompanied by lower N/P, reflects the species succession and prevalence of diatoms in the phytoplankton assemblage. The lower N/P uptake ratios coinciding with near depleted NO_3 concentrations suggests that intense nitrogen recycling occurred in the mixed layer and that other sources of nitrogen, such as ammonium, could be important to sustain phytoplankton production. The variable NO_3 (and PO_4) concentrations below the mixed layer integrate the effects of uptake by phytoplankton in surface waters and regeneration from remineralisation of sinking organic matter and mixing with underlying waters. Due to the shallowing seafloor towards the inner fjord and deep convective mixing, a substantial fraction of organically fixed carbon and nutrients (and exported silicates) is likely respired and returned to the water column. This mechanism would resupply the surface layers with NO_3, and possibly iron, to maintain biological production and induce high seasonality of C_T and likely lower the potential for organic carbon burial in the sediments (Smith et al., 2015) in the inner fjord.

Surface waters were undersaturated with respect to atmospheric CO_2, but oceanic CO_2 uptake of 3.9 ± 0.3 g C m^{-2} yr^{-1}, estimated for the full annual cycle, would resupply the upper layers with C_T. However, a net monthly decrease in the deficit in C_T is observed due to the dominating effects of freshwater inputs and NCP. The growing season NCP_C estimate for Kaldfjorden (14 ± 2 g C m^{-2}) is smaller compared to carbon-based NCP estimates of 49 g C m^{-2} for the Amundsen Gulf region (Shadwick et al., 2011) and 65–85 g C m^{-2} in Adventfjorden in Svalbard (Ericson et al., 2019a). The seasonal NCP_C is slightly less than the equivalent $NCP_{N,P}$ estimates for the Nordic and Barents seas and Canadian Archipelago of 30–40 g C m^{-2} (Codispoti et al., 2013). The annual NCP_C estimates for Kaldfjorden (5 ± 2 g C m^{-2} yr^{-1}) are modest in comparison to the carbon-based NCP estimates of 34 g C m^{-2} yr^{-1} in Adventfjorden in Svalbard (Ericson et al., 2019b) and 108 g C m^{-2} yr^{-1} in the Fram Strait–Svalbard region (Vaquer-Sunyer et al., 2013). These variations show enhanced seasonal and annual NCP in the higher latitude Arctic regions, likely due to higher productivity in sea-ice-influenced areas, enhanced oceanic exchanges for nutrient resupply, and greater export of organic matter from the productive surface layer to subsurface waters.

Accounting for freshwater effects, mixing and NCP, the remaining seasonal variations in surface water C_T can be attributed to air–sea CO_2 exchange and residual changes that integrate variations in A_T, such as calcium carbonate formation/dissolution. To investigate this scenario, potential alkalinity (A_T*) was evaluated to show that the water column average was 2285 ± 12 μmol kg^{-1} with largest variations across the fjord from July to October (**Figure 14b**). Decreases in surface water A_T* of ~50 μmol kg^{-1} are indicative of $CaCO_3$ formation during biogenic calcification, which was most pronounced from July to September. This period encompassed the summer phytoplankton bloom, when bloom-forming coccolithophores disturb the optical properties of surface waters and can be detected by signals in light reflectance by remote sensing (Tyrrell et al., 1999). Coccolithophores are widely abundant in the global oceans and influence seawater carbonate chemistry through the synthesis of $CaCO_3$ shells. The $CaCO_3$, or particulate inorganic carbon, that is exported out of the surface can either dissolve upon transport to deeper water layers or become buried in sediments (Rost and Riebesell, 2004). MODIS-Aqua satellite-corrected reflectance available from NASA Worldview shows development of a coccolithophore bloom in Kaldfjorden during this study (**Figure 15**). Images taken at the time of each sampling event (8 June, 25 July, 6 September), or those closest in time that are not obscured by cloud cover, and the 1st of each month show the bloom extended across Kaldfjorden by 26 July until 26 August. No reflectance in clear water was seen by the next sampling event on 6 September.

These observations support the proposed mechanism of removal of A_T by calcification (and concomitant reduction in monthly $\Delta C_{T\,CaCO_3}$), which would equate to a drawdown in C_T of ~25 μmol kg^{-1}. The $\Delta C_{T\,bio\,C}$ accounts for about 20% of the $\Delta C_{T\,total}$ and $\Delta C_{T\,alk}$ made a minor contribution (up to 8%) to $\Delta C_{T\,total}$, which shows the importance of calcifying phytoplankton in carbon cycling in the region. In the following autumn months, increases in A_T* up to 40 μmol kg^{-1} (positive $\Delta C_{T\,alk}$) indicated A_T inputs from terrestrial weathering and perhaps from $CaCO_3$ dissolution in a decaying coccolithophore bloom, likely from sampling events that captured particulate inorganic carbon ($CaCO_3$ shells) in the water column.

Ocean acidification state and CO_2 uptake

The water column across Kaldfjorden remained saturated with respect to aragonite (and calcite, not shown) during the study period. The annual Ω range in Kaldfjorden compares very well (1.3–2.5) to that reported for fjords of western Norway (Omar et al., 2016). Seasonality in surface water Ω from minima in winter/spring to maximum in late summer was driven by changes in C_T from the production (photosynthesis) and decay (respiration/remineralisation) of organic matter. Over the growing season, biological production reduced C_T by 100 μmol kg^{-1} in surface waters, leading to concomitant increases in Ω to 2.26–2.33 from March to September. Increases in $\Delta\Omega_{bio\,C}$ (and $\Delta\Omega_{bio\,N}$) of 0.25–0.40 between April to June dominated the monthly

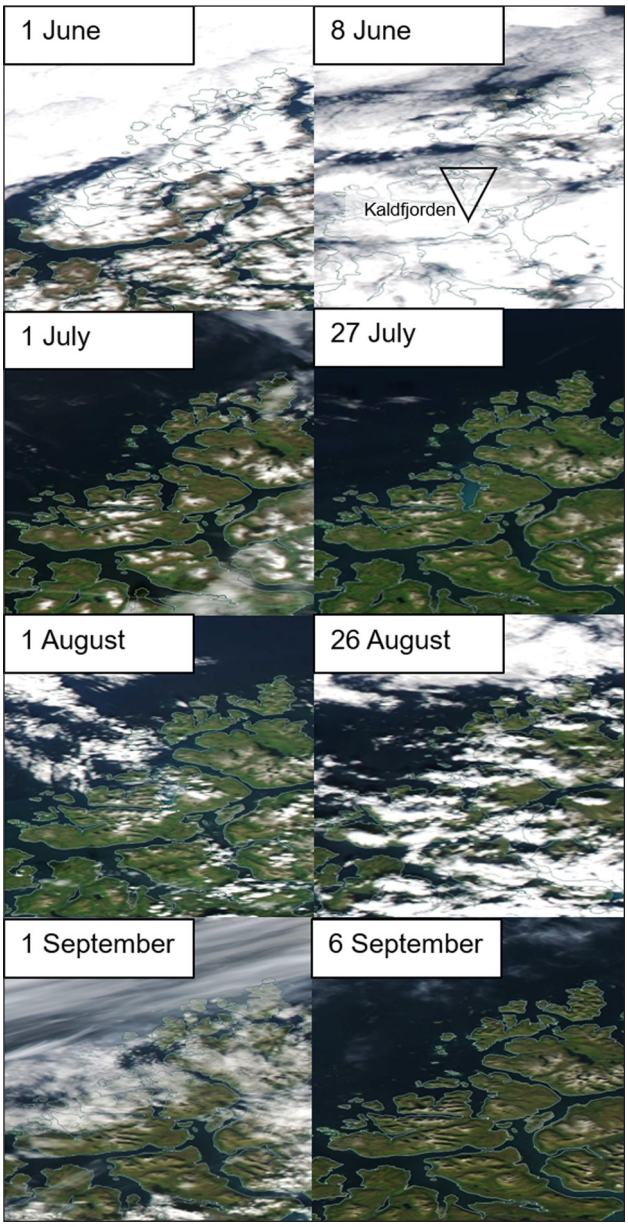

Figure 15: Satellite reflectance in the Kaldfjorden region from June to September 2018. The temporal variations in surface water reflectance from MODIS Aqua satellite as a proxy for marine carbonates as coccolithophores from images obtained on 1 June, 1 July, 1 August, 1 September and cloud-free days on 8 June, 27 July, 26 August and 6 September during/close to sampling events. The location of Kaldfjorden is marked by a black triangle on the 8 June image. DOI: https://doi.org/10.1525/elementa.438.f15

changes Ω to show the importance of biological carbon uptake on the surface water acidification state (**Figure 12**). Removal of A_T and subsequent lowering of Ω during calcification constituted a minor competing effect ($\Delta\Omega_{CaCO_3}$ of –0.09) that slightly counteracted the biologically-driven increases in Ω from C_T drawdown in summer coccolithophore blooms. The effect of freshwater dilution reducing C_T largely offset the parallel effect of A_T reduction, resulting in increases in $\Delta\Omega_{sal}$ up to 0.11 across the fjord during the period of increasing freshwater fractions (April to June). Photosynthetically driven increases in Ω that counteract effects of freshwater dilution have been reported in other high latitude coast and fjord regions (Chierici and Fransson, 2009; Chierici et al., 2011; Fransson et al., 2015, 2016; Ericson et al., 2019a). The decrease in Ω to ~1.9 from May to June 2018 coincided with an episodic drop in salinity during a period of precipitation and peak freshwater fractions. Concomitant decreases in $\Delta\Omega_{bio\ C}$ and $\Delta\Omega_{flux}$ suggested that suppression of Ω had occurred through increased C_T from the degradation of organic matter and atmospheric CO_2 uptake in the freshwater flowing into the fjord, as previously reported (Anderson et al., 2009; Shadwick et al., 2011; Evans et al., 2014; Meire et al., 2015; Ericson et al., 2018). In addition, changes in water temperature affect Ω as colder waters have lower carbonate saturation through thermodynamic controls; increases in Ω by 1% arise due to warming of 1°C (Mucci, 1983). Coldest surface waters (2.17°C) with Ω of 1.59 in March warmed by 10.1°C to seasonal maximum (12.27°C) with Ω of 2.10 in July; thus, a thermodynamic increase in Ω of 0.16 could be expected and contribute to positive $\Delta\Omega_{total}$ during this time. Saturation states steadily decreased during the autumn, winter and early spring in post-bloom conditions driven by organic matter remineralisation and net respiration ($\Delta\Omega_{bio\ C}$ of –0.50) with effects of seasonal cooling. Impacts of mixing with subsurface carbon-rich Norwegian Coastal Water and air–sea CO_2 exchange played minor roles in monthly changes in Ω in surface waters.

Throughout each season, surface waters remained undersaturated with respect to the atmosphere and showed that Kaldfjorden was a sink for atmospheric CO_2 on an annual basis. Previous studies have also reported net atmospheric CO_2 sinks for sub-Arctic coast and fjord systems (Omar et al., 2016; Tynan et al., 2016; Yasunaka et al., 2016). The mean atmospheric CO_2 uptake of 0.86 ± 0.63 mmol m^{-2} day^{-1} is similar to that of 0.73 ± 0.40 mmol m^{-2} day^{-1} estimated for a marginal Arctic coastal environment of Hudson Bay, Canada (Else et al., 2008b). Wind speeds in Kaldfjorden were dampened due to orographic steering, compared to measurements off the shelf (Nordby et al., 1999); thus, atmospheric CO_2 uptake in Kaldfjorden of 2.7 mmol m^{-2} day^{-1} is weak compared with the CO_2 influx of >15 mmol m^{-2} day^{-1} for the Norwegian Sea (Yasunaka et al., 2016) and the non-ice-covered Arctic shelf seas that generally absorb CO_2 at between 1 and 15 mmol m^{-2} day^{-1} (Omar et al., 2005; Cai et al., 2006; Else et al., 2008a, 2013; Ericson et al., 2018; Chierici et al., 2019). Enhanced CO_2 uptake in higher latitude waters results from substantial blooms, greater biological productivity and subsequent export of organic matter to deeper waters, coupled to strong winds enhancing oceanic CO_2 uptake. These results highlight the large spatial variability of the oceanic CO_2 sink and emphasize the need to resolve key processes on regional scales.

Fjords in the future

Strong seasonality in hydrography, carbonate chemistry, and macronutrients in the marine environment of Kaldfjorden, northern Norway, was driven by freshwater

inputs, biological production, and mixing with subsurface coastal water. High latitude fjord and coastal environments may be particularly sensitive to future changes in ocean chemistry and the effects of ocean acidification, compared to the open ocean, due to the greater influence and spatial-temporal variations of freshwater sources and terrestrial influences. Fjords are dynamic ecosystems that naturally experience large ranges in carbonate chemistry and thus may exhibit a degree of resilience to future changes but may also be vulnerable to extreme values. Freshwater inputs play a key role in monthly changes in the acidification state (Ω) of surface waters through dilution effects on C_T and A_T. Increases in air and seawater temperatures and greater freshwater fluxes will have consequences for the seasonal stratification and mixing of the water column, as well as phytoplankton species composition, bloom development, and biogeochemical cycling. Freshwater entering the fjord changes the seawater chemistry so that A_T, carbonate ion concentrations and pH decrease due to dilution. In addition to continued uptake of anthropogenic CO_2, these processes reduce the buffering capacity of the fjord water and increase the vulnerability of surface waters to acidification. Increased acidification is expected to have adverse effects on marine life, such as the pelagic calcifiers, coccolithophores, which contribute to monthly C_T deficits during summer blooms and form an integral part of the food web (Andersson et al., 2015). Terrestrial inputs of organic matter and weathered minerals, such as carbonates and silicates from the surrounding bedrock (Fransson et al., 2015), enhance C_T and provide a minor source of A_T to surface waters. Effects of dilution from freshwater were strongly counteracted by primary production, with intense C_T and nitrate drawdown from the period of the spring bloom to early autumn dominating the Ω seasonality. Estimates of NCP were modest but in accordance with other high latitude fjord and coastal regions: Kaldfjorden is an annual sink for atmospheric CO_2. High latitude fjords have been regarded as regions of high organic carbon sequestration, provided strong stratification does not prevail during the productive season, and if elevated fluxes of organic matter from productive surface waters and surrounding terrestrial sources can be exported and stored in fjord sediments (Smith et al., 2015). Changes in pH may also influence other chemical processes such as bioavailability of metals and toxins (Millero et al., 2009; Breitbarth et al., 2010).

The time-series data presented here emphasise the need for year-round sampling to better understand the natural variability in the marine environment. Addressing some of the remaining uncertainties could include resolving the characteristics (C_T, A_T, nutrients, $\delta^{18}O$, salinity, organic matter) of the oceanic (coastal) and freshwater endmembers to elucidate the main sources of inorganic and organic carbon, nutrients and minerals to Kaldfjorden. Phytoplankton community composition and net primary production, as well as drawdown of carbon and uptake of atmospheric CO_2, will ultimately depend on how the fjord marine ecosystems will respond to climatically induced changes. Observations of the biogeochemical dynamics on seasonal timescales further our understanding of carbon and nutrient cycling in these important marine systems and serve as benchmarks against which future changes can be compared and evaluated.

Data Accessibility Statement

The data collected during this study are publicly available at the Norwegian Marine Data Centre with the following reference Angelika Renner (2020) Hydrography in Kaldfjorden, Troms, Norway. DOI: 10.21335/NMDC-1539462099.

Acknowledgements

The authors gratefully acknowledge the Captains and crews of RV *Helmer Hanssen*, RV *Johan Hjort*, RV *Johan Ruud* and RV *Kronprins Haakon* for the logistical support and opportunity to use the vessels to conduct fieldwork. Particular thanks to Z Walker (UW/UiT), K Dunlop (IMR), P Renaud (Akvaplan-niva), C Ballantine (Akvaplan-niva) and KØ Gjelland (NINA) for boat logistics and use of Dytiscus and numerous others for assistance with boating and sample collection. We would like to thank the Editors and two reviewers for valuable comments that have helped to greatly improve the manuscript.

Funding information

This work was part of the project "Impact of massive Winter Herring Abundances on the KaLdfjorden Environment (WHALE; grant number 201914747042018), which was funded by the flagship "Effects of climate change on sea and coastal ecology in the north" and the flagship "Ocean acidification and effects in northern waters" of the FRAM – High North Research Centre for Climate and the Environment. I Wiedmann was funded by ARCEx, the Research Centre for Arctic Petroleum Exploration (Norwegian Research Council #228107 and industry partners).

Competing interests

The authors have no competing interests to declare.

Author contributions

- Contributed to conception and design: AR, IW, MC, MB
- Contributed to acquisition of data: AR, EJ, MB, HHL
- Contributed to analysis and interpretation of data: EJ, HHL, AR, IW, MC
- Drafted and/or revised the article: EJ, AR, IW, MC
- Approved the submitted version for publication: EJ, AR, IW, MC, HHL, MB

References

Albretsen, J, Aure, J, Sætre, R and **Danielssen, DS.** 2012. Climatic variability in the Skagerrak and coastal waters of Norway. *ICES J Mar Sci* **69**(5): 758–763. DOI: https://doi.org/10.1093/icesjms/fsr187

Ambrose, D and **Lawrenson, IJ.** 1972. The vapor pressure of water. *The Journal of Chemical Thermodynamics* **4**(5): 755–761. DOI: https://doi.org/10.1016/0021-9614(72)90049-3

Anderson, LG, Jutterström, S, Hjalmarsson, S, Wåhlström, I and **Semiletov, IP.** 2009. Out-gassing of CO_2 from Siberian Shelf seas by terrestrial organic

matter decomposition. *Geophys Res Lett* **36**: L20601. DOI: https://doi.org/10.1029/2009GL040046

Andersson, AJ, Kline, DI, Edmunds, PJ, Archer, SD, Bednaršek, N, Carpenter, RC, Chadsey, M, Goldstein, P, Grottoli, AG, Hurst, TP, King, AL, Kübler, JE, Kuffner, IB, Mackey, KRM, Menge, BA, Paytan, A, Riebesell, U, Schnetzer, A, Warner, ME and **Zimmerman, RC.** 2015. Understanding ocean acidification impacts on organismal to ecological scales. *Oceanography* **28**(2): 16–27. DOI: https://doi.org/10.5670/oceanog.2015.27

Arrigo, KR. 2005. Marine microorganisms and global nutrient cycles. *Nature* **437**(7057): 349–355. DOI: https://doi.org/10.1038/nature04159

Asplin, L, Johnsen, IA, Sandvik, AD, Albretsen, J, Sundfjord, V, Aure, J and **Boxaspen, KK.** 2014. Dispersion of salmon lice in the Hardangerfjord. *Mar Biol Res* **10**: 216–225. DOI: https://doi.org/10.1080/17451000.2013.810755

Aure, J and **Stigebrandt, A.** 1989. On the influence of topographic factors upon the oxygen consumption rate in sill basins of fjords. *Estuar Coast Shelf Sci* **28**: 59–69. DOI: https://doi.org/10.1016/0272-7714(89)90041-3

Azetsu-Scott, K, Starr, M, Mei, Z-P and **Granskog, M.** 2014. Low calcium carbonate saturation state in an Arctic inland sea having large and varying fluvial inputs: The Hudson Bay system. *J. Geophys. Res. Oceans* **119**: 6210–6220. DOI: https://doi.org/10.1002/2014JC009948

Borges, AV. 2005. Do we have enough pieces of the jigsaw to integrate CO_2 fluxes in the coastal ocean? *Estuaries* **28**: 3–27. DOI: https://doi.org/10.1007/BF02732750

Bourgeois, T, Orr, JC, Resplandy, L, Terhaar, J, Ethé, C, Gehlen, M and **Bopp, L.** 2016. Coastal-ocean uptake of anthropogenic carbon. *Biogeosciences* **13**: 4167–4185. DOI: https://doi.org/10.5194/bg-13-4167-2016

Bozec, Y, Thomas, H, Schiettecatte, L-S, Borges, AV, Elkalay, K and **de Baar, HJW.** 2006. Assessment of the processes controlling the seasonal variations of dissolved inorganic carbon in the North Sea. *Limnol Oceanogr* **51**: 2746–2762. DOI: https://doi.org/10.4319/lo.2006.51.6.2746

Brattegard, T, Høisæter, T, Sjøtun, K, Fenchel, T and **Uiblein, F.** 2011. Norwegian fjords: From natural history to ecosystem ecology and beyond. *Mar Biol Res* **7**: 421–424. DOI: https://doi.org/10.1080/17451000.2011.561355

Breitbarth, E, Bellerby, RJ, Neill, CC, Ardelan, MV, Meyerhöfer, M, Zöllner, E, Croot, PL and **Riebesell, U.** 2010. Ocean acidification affects iron speciation during a coastal seawater mesocosm experiment. *Biogeosci* **7**: 1065–1073. DOI: https://doi.org/10.5194/bg-7-1065-2010

Brewer, PG and **Goldman, JC.** 1976. Alkalinity changes generated by phytoplankton growth. *Limnol Ocean* **21**: 108–117. DOI: https://doi.org/10.4319/lo.1976.21.1.0108

Burt, WJ, Thomas, H, Miller, LA, Granskog, MA, Papakyriakou, TN and **Pengelly, L.** 2016. Inorganic carbon cycling and biogeochemical processes in an Arctic inland sea (Hudson Bay). *Biogeosci* **13**: 4659–4671. DOI: https://doi.org/10.5194/bg-13-4659-2016

Cai, W-J. 2011. Estuarine and coastal ocean carbon paradox: CO_2 sinks or sites of terrestrial carbon incineration? *Ann. Rev. Mar. Sci.* **3**: 123–145. DOI: https://doi.org/10.1146/annurev-marine-120709-142723

Cai, W-J, Dai, M and **Wang, Y.** 2006. Air–sea exchange of carbon dioxide in ocean margins: a province-based synthesis. *Geophys Res Lett* **33**: L12603. DOI: https://doi.org/10.1029/2006GL026219

Chavez, FP, Takahashi, T, Cai, W-J, Friederich, G, Hales, B, Wanninkhof, R and **Feely, RA.** 2007. Coastal Oceans. In: *The First State of the Carbon Cycle Report (SOCCR)*, King, AW, Dilling, L, Zimmerman, GP, Fairman, DM, Houghton, RA, Marland, GH, Rose, AZ, Wilbanks, TJ (eds.). Asheville, NC: NOAA, Natl. Clim. Data Cent., 157–166.

Chen, B, Cai, W-J and **Chen, L.** 2015. The marine carbonate system of the Arctic Ocean: assessment of internal consistency and sampling considerations, summer 2010. *Mar Chem* **176**: 174–188. DOI: https://doi.org/10.1016/j.marchem.2015.09.007

Chen, C-TA and **Borges, AV.** 2009. Reconciling opposing views on carbon cycling in the coastal ocean: continental shelves as sinks and near-shore ecosystems as sources of atmospheric CO_2. *Deep-Sea Res II* **56**: 578–90. DOI: https://doi.org/10.1016/j.dsr2.2009.01.001

Chierici, M and **Fransson, A.** 2009. Calcium carbonate saturation in the surface water of the Arctic Ocean: undersaturation in freshwater influenced shelves. *Biogeosci* **6**: 2421–2432. DOI: https://doi.org/10.5194/bg-6-2421-2009

Chierici, M, Fransson, A, Lansard, B, Miller, LA, Mucci, A, Shadwick, E, Thomas, H, Tremblay, J-E and **Papakyriakou, TN.** 2011. Impact of biogeochemical processes and environmental factors on the calcium carbonate saturation state in the Circumpolar Flaw Lead in the Amundsen Gulf, Arctic Ocean. *J Geophys Res* **116**: C00G09. DOI: https://doi.org/10.1029/2011JC007184

Chierici, M, Vernet, M, Fransson, A and **Børsheim, KY.** 2019. Net community production and carbon exchange from winter to summer in the Atlantic water inflow to the Arctic Ocean. *Front Mar Sci* **6**: 528. DOI: https://doi.org/10.3389/fmars.2019.00528

Codispoti, LA, Kelly, V, Thessen, A, Matrai, P, Suttles, S, Hill, V, Steele, M and **Light, B.** 2013. Synthesis of primary production in the Arctic Ocean: III. Nitrate and phosphate based estimates of net community production. *Prog Oceanogr* **110**: 126–150. DOI: https://doi.org/10.1016/j.pocean.2012.11.006

Cooper, LW, McClelland, JW, Holmes, RM, Raymond, PA, Gibson, JJ, Guay, CK and **Peterson, BJ.** 2008. Flow-weighted values of runoff tracers ($\delta^{18}O$, DOC, Ba, alkalinity) from the six largest Arctic rivers.

Geophys Res Lett **35**: L18606. DOI: https://doi.org/10.1029/2008GL035007

Cottier, FR, Nilsen, F, Skogseth, R, Tverberg, V, Skarðhamar, J and **Svendsen, H.** 2010. Arctic fjords: a review of the oceanographic environment and dominant physical processes. *Geological Society, London, Special Publications* **344**(1): 35–50. DOI: https://doi.org/10.1144/SP344.4

Dickson, AG and **Millero, FJ.** 1987. A comparison of the equilibrium constants for the dissociation of carbonic acid in seawater media. *Deep Sea Res Part A* **34**(10): 1733–1743. DOI: https://doi.org/10.1016/0198-0149(87)90021-5

Dickson, AG, Sabine, CL and **Christian, JR.** (eds.) 2007. Guide to best practices for ocean CO_2 measurements. *PICES Special Publication* **3**: 191.

Doney, SC, Balch, WM, Fabry, VJ and **Feely, RA.** 2009. Ocean acidification: a critical emerging problem for the ocean sciences. *Oceanography* **22**(4): 16–25. DOI: https://doi.org/10.5670/oceanog.2009.93

Erga, SR and **Heimdal, BR.** 1984. Ecological studies on the phytoplankton of Korsfjorden, western Norway. The dynamics of a spring bloom seen in relation to hydrographical conditions and light regime. *J Plankt Res* **6**(1): 67–90. DOI: https://doi.org/10.1093/plankt/6.1.67

Eilertsen, HC and **Degerlund, M.** 2010. Phytoplankton and light during the northern high-latitude winter. *J Plankton Res* **32**(6): 899–912. DOI: https://doi.org/10.1093/plankt/fbq017

Eilertsen, HC and **Frantzen, S.** 2007. Phytoplankton from two sub-Arctic fjords in Northern Norway 2002–2004: I. Seasonal variations in chlorophyll *a* and bloom dynamics. *Mar Biol Res* **3**(5): 319–332. DOI: https://doi.org/10.1080/17451000701632877

Eilertsen, HC, Schei, B and **Taasen, JP.** 1981. Investigations on the plankton community of Balsfjorden, Northern Norway. The phytoplankton 1976–1978. Abundance, species composition, and succession. *Sarsia* **66**: 129–141. DOI: https://doi.org/10.1080/00364827.1981.10414530

Eilertsen, HC and **Taasen, JP.** 1984. Investigations on the plankton community of Balsfjorden, Northern Norway. The phytoplankton 1976–1978. Environmental factors, dynamics of growth, and primary production. *Sarsia* **69**: 1–15. DOI: https://doi.org/10.1080/00364827.1984.10420584

Else, BGT, Papakyriakou, TN, Asplin, MG, Barber, DG, Galley, RJ, Miller, LA and **Mucci, A.** 2013. Annual cycle of air–sea CO_2 exchange in an Arctic Polynya region. *Glob Biogeochem Cycles* **27**: 388–398. DOI: https://doi.org/10.1002/gbc.20016

Else, BGT, Papakyriakou, TN, Granskog, MA and **Yackel, JJ.** 2008b. Observations of sea surface fCO_2 distributions and estimated air–sea CO_2 fluxes in the Hudson Bay region (Canada) during the open water season. *J Geophys Res* **113**: C08026. DOI: https://doi.org/10.1029/2007JC004389

Else, BGT, Yackel, JJ and **Papakyriakou, TN.** 2008a. Application of satellite remote sensing techniques for estimating air–sea CO_2 fluxes in Hudson Bay, Canada during the ice–free season. *Remote Sens Environ* **112**: 3550–3562. DOI: https://doi.org/10.1016/j.rse.2008.04.013

Ericson, Y, Chierici, M, Falck, E, Fransson, A, Jones, EM and **Kristiansen, S.** 2019b. Seasonal dynamics of the marine CO_2 system in Adventfjorden, a West Spitsbergen fjord. *Polar Research* **38**: 3345. DOI: https://doi.org/10.33265/polar.v38.3345

Ericson, Y, Falck, E, Chierici, M, Fransson, A and **Kristiansen, S.** 2019a. Marine CO_2 system variability in a high arctic tidewater-glacier fjord system, Tempelfjorden, Svalbard. *Cont Shelf Res* **181**: 1–13. DOI: https://doi.org/10.1016/j.csr.2019.04.013

Ericson, Y, Falck, E, Chierici, M, Fransson, A, Kristiansen, S, Platt, SM, Hermansen, O and **Myhre, CL.** 2018. Temporal variability in surface water $\boldsymbol{p}CO_2$ in Adventfjorden (West Spitsbergen) with emphasis on physical and biogeochemical drivers. *J Geophys Res Oceans* **123**: 4888–4905. DOI: https://doi.org/10.1029/2018JC014073

Evans, W, Mathis, JT and **Cross, JN.** 2014. Calcium carbonate corrosivity in an Alaskan inland sea. *Biogeosci* **11**: 365–379. DOI: https://doi.org/10.5194/bg-11-365-2014

Evans, W, Mathis, JT, Cross, JN, Bates, NR, Frey, KE, Else, BGT, Papkyriakou, TN, DeGrandpre, MD, Islam, F, Cai, W-J, Chen, B, Yamamoto-Kawai, M, Carmack, E, Williams, WJ and **Takahashi, T.** 2015. Sea–air CO_2 exchange in the western Arctic coastal ocean. *Global Biogeochem Cy.* **29**: 1190–1209. DOI: https://doi.org/10.1002/2015GB005153

Fabry, VJ, McClintock, JB, Mathis, JT and **Grebmeier, JM.** 2009. Ocean acidification at high latitudes: The bellwether. *Oceanography* **22**(4): 160–171. DOI: https://doi.org/10.5670/oceanog.2009.105

Fabry, VJ, Seibel, BA, Feely, RA and **Orr, JC.** 2008. Impacts of ocean acidification on marine fauna and ecosystem processes. *ICES J Mar Sci* **65**(3): 414–432. DOI: https://doi.org/10.1093/icesjms/fsn048

Fennel, K, Alin, S, Barbero, L, Evans, W, Bourgeois, T, Cooley, S, Dunne, J, Feely, RA, Hernandez-Ayon, JM, Hu, X, Lohrenz, S, Muller-Karger, F, Najjar, R, Robbins, L, Shadwick, E, Siedlecki, S, Steiner, N, Sutton, A, Turk, D, Vlahos, P and **Wang, ZA.** 2019. Carbon cycling in the North American coastal ocean: a synthesis. *Biogeosciences* **16**: 1281–1304. DOI: https://doi.org/10.5194/bg-16-1281-2019

Fosså, JH, Mortensen, PB and **Furevik, DM.** 2002. The deep-water coral *Lophelia pertusa* in Norwegian waters: distribution and fishery impacts. *Hydrobiologia* **471**: 1–12. DOI: https://doi.org/10.1023/A:1016504430684

Fransson, A, Chierici, M, Hop, H, Findlay, HS, Kristiansen, S and **Wold, A.** 2016. Late winter-to-summer change in ocean acidification state in Kongsfjorden, with implications for calcifying organisms. *Polar Biol* **39**(10): 1841–1857. DOI: https://doi.org/10.1007/s00300-016-1955-5

Fransson, A, Chierici, M, Miller, LA, Carnat, G, Shadwick, E, Thomas, H, Pineault, S and **Papakyriakou, TN.** 2013. Impact of sea-ice processes on the carbonate system and ocean acidification at the ice–water interface of the Amundsen Gulf, Arctic Ocean. *J Geophys Res Oceans* **118**: 7001–7023. DOI: https://doi.org/10.1002/2013JC009164

Fransson, A, Chierici, M, Nomura, D, Granskog, MA, Kristiansen, S, Martma, T and **Nehrke, G.** 2015. Effect of glacial drainage water on the CO_2 system and ocean acidification state in an Arctic tidewater-glacier fjord during two contrasting years. *J Geophys Res Oceans* **120**: 2413–2429. DOI: https://doi.org/10.1002/2014JC010320

Frigstad, H, Andersen, T, Bellerby, RGJ, Silyakova, A and **Hessen, DO.** 2014. Variation in the seston C:N ratio of the Arctic Ocean and pan-Arctic shelves. *J Mar Sys* **129**: 214–223. DOI: https://doi.org/10.1016/j.jmarsys.2013.06.004

Friis, K, Körtzinger, A and **Wallace, DWR.** 2003. The salinity normalization of marine inorganic carbon chemistry data. *Geophys Res Lett* **30**: 1085. DOI: https://doi.org/10.1029/2002GL015898

Grasshoff, K, Kremling, K and **Ehrhardt, M.** 2009. *Methods of Seawater Analysis*, 3rd Edn. New York, NY: John Wiley.

Grønvik, S and **Hopkins, CCE.** 1984. Ecological investigations of the zooplankton community of Balsfjorden, Northern Norway: Generation cycle, seasonal vertical distribution, and seasonal variations in body weight and carbon and nitrogen content of the copepod *Metridia longa* (Lubbock). *J Exp Mar Biol Ecol* **80**(1): 93–107. DOI: https://doi.org/10.1016/0022-0981(84)90096-0

Gruber, N and **Sarmiento, JL.** 1997. Global patterns of marine nitrogen fixation and denitrification. *Glob Biogeochem Cy* **11**: 235–266. DOI: https://doi.org/10.1029/97GB00077

Hartman, B and **Hammond, DE.** 1985. Gas exchange in San Francisco Bay. *Hydrobiologia* **129**: 59–68. DOI: https://doi.org/10.1007/BF00048687

Hjalmarsson, S, Wesslander, K, Anderson, LG, Omstedt, A, Perttilä, M and **Mintrop, L.** 2008. Distribution, long-term development and mass balance calculation of total alkalinity in the Baltic Sea. *Cont Shelf Res* **28**: 593–601. DOI: https://doi.org/10.1016/j.csr.2007.11.010

Inall, ME and **Gillibrand, PA.** 2010. The physics of mid-latitude fjords: a review. *Geological Society, London, Special Publications* **344**(1): 17–33. DOI: https://doi.org/10.1144/SP344.3

Johnson, KM, Sieburth, JM, leB Williams, PJ and **Brändström, L.** 1987. Coulometric total carbon dioxide analysis for marine studies: automation and calibration. *Mar Chem* **21**: 117–133. DOI: https://doi.org/10.1016/0304-4203(87)90033-8

Jones, E, Chierici, M, Skjelvan, I, Norli, M, Børsheim, KY, Lødemel, HH, Kutti, T, Sørensen, K, King, AL, Lauvset, S, Jackson, K, de Lange, T, Johannsessen, T and **Mourgues, C.** 2019. Monitoring ocean acidification in Norwegian Seas in 2018, Rapport, Miljødirektoratet, M-1417|2019.

Kähler, P and **Koeve, W.** 2001. Marine dissolved organic matter: can its C:N ratio explain carbon overconsumption? *Deep Sea Res I* **48**: 49–62. DOI: https://doi.org/10.1016/S0967-0637(00)00034-0

Keck, A and **Wassmann, P.** 1996. Temporal and spatial patterns of sedimentation in the subarctic fjord Malangen, Northern Norway. *Sarsia*, **80**(4): 259–276. DOI: https://doi.org/10.1080/00364827.1996.10413600

Klinck, JM, O'Brien, JJ and **Svendsen, H.** 1981. A simple model of fjord and coastal circulation interaction. *J Phys Ocean* **11**(12): 1612–1626. DOI: https://doi.org/10.1175/1520-0485(1981)011<1612:ASMOFA>2.0.CO;2

Laruelle, GG, Lauerwald, R, Pfeil, B and **Regnier, P.** 2014. Regionalized global budget of the CO_2 exchange at the air-water interface in continental shelf seas. *Global Biogeochem Cy* **28**: 1199–1214. DOI: https://doi.org/10.1002/2014GB004832

Lauvset, SK, Gruber, N, Landschützer, P, Olsen, A and **Tjiputra, J.** 2015. Trends and drivers in global surface ocean pH over the past 3 decades. *Biogeosci* **12**: 1285–1298. DOI: https://doi.org/10.5194/bg-12-1285-2015

Lewis, E and **Wallace, DWR.** 1998. Program developed for CO_2 system calculations. *ORNL/CDIAC-105.* Oak Ridge, TN: Carbon Dioxide Information Analysis Center, Oak Ridge National Laboratory, US Department of Energy. DOI: https://doi.org/10.15485/1464255

Matthews, JBL and **Sands, NJ.** 1973. Ecological studies on the deep-water pelagic community of Korsfjorden, western Norway. The topography of the area and its hydrography in 1968–1972, with a summary of the sampling programmes. *Sarsia* **52**: 29–52. DOI: https://doi.org/10.1080/00364827.1973.10411230

Meire, L, Søgaard, DH, Mortensen, J, Meysman, FJR, Soetaert, K, Arendt, KE, Juul-Pedersen, T, Blicher, ME and **Rysgaard, S.** 2015. Glacial meltwater and primary production are drivers of strong CO_2 uptake in fjord and coastal waters adjacent to the Greenland Ice Sheet. *Biogeosci* **12**: 2347–2363. DOI: https://doi.org/10.5194/bg-12-2347-2015

Mehrbach, C, Culberson, CH, Hawley, JE and **Pytkowicz, RM.** 1973. Measurement of the apparent dissociation constants of carbonic acid in seawater at atmospheric pressure. *Limnol Oceanog* **18**: 897–907. DOI: https://doi.org/10.4319/lo.1973.18.6.0897

Michelsen, HK, Svensen, C, Reigstad, M, Nilssen, EM and **Pedersen, T.** 2017. Seasonal dynamics of meroplankton in a high-latitude fjord. *J Mar Sys* **168**: 17–30. DOI: https://doi.org/10.1016/j.jmarsys.2016.12.001

Millero, FJ and **Leung, WH.** 1976. The thermodynamics of seawater at one atmosphere. *Am J Sci* **276**(9): 1035–1077. DOI: https://doi.org/10.2475/ajs.276.9.1035

Millero, FJ, Woosley, R, DiTrolio, B and **Waters, J.** 2009. Effect of ocean acidification on the speciation of metals in seawater. *Oceanography* **22**(4): 72–85. DOI: https://doi.org/10.5670/oceanog.2009.98

Mucci, A. 1983. The solubility of calcite and aragonite in seawater at various salinities, temperatures, and one atmosphere total pressure. *Am J Sci* **283**: 780–799. DOI: https://doi.org/10.2475/ajs.283.7.780

Myksvoll, MS, Sandvik, AD, Skarðhamar, J and **Sundby, S.** 2012. Importance of high resolution wind forcing on eddy activity and particle dispersion in a Norwegian fjord. *Estuar Coast Shelf Sci* **113**: 293–304. DOI: https://doi.org/10.1016/j.ecss.2012.08.019

Noji, TT, Noji, CI-M and **Barthel, K-G.** 1993. Pelagic-benthic coupling during the onset of winter in a Northern Norwegian fjord. Carbon flow and fate of suspended particulate matter. *Mar Ecol Progr Ser* **93**(1–2): 89–99. DOI: https://doi.org/10.3354/meps093089

Nordby, E, Tande, KS, Svendsen, H, Slagstad, D and **Båmstedt, U.** 1999. Oceanography and fluorescence at the shelf break off the north Norwegian coast (69°′N–70°30′N) during the main productive period in 1994. *Sarsia* **84**: 175–189. DOI: https://doi.org/10.1080/00364827.1999.10420424

Omar, A, Johannessen, T, Bellerby, RGJ, Olsen, A, Anderson, LG and **Kivimäe, C.** 2005. Sea-ice brine formation in Storfjorden: Implications for the Arctic wintertime air–sea CO_2 flux. In: *The Nordic Seas: An integrated perspective. Geophysical Monograph Series 158*, Drange, H, Dokken, T, Furevik, T, Gerdes, R and Berger, W (eds.), 177–187. Washington, DC: AGU. DOI: https://doi.org/10.1029/158GM12

Omar, AM, Skjelvan, I, Erga, SR and **Olsen, A.** 2016. Aragonite saturation states and pH in western Norwegian fjords: seasonal cycles and controlling factors, 2005–2009. *Ocean Sci* **12**: 937–951. DOI: https://doi.org/10.5194/os-12-937-2016

Orr, JC, Fabry, VJ, Aumont, O, Bopp, L, Doney, SC, Feely, RA, Gnanadesikan, A, Gruber, N, Ishida, A, Joos, F, Key, RM, Lindsay, K, Maier-Reimer, E, Matear, R, Monfray, P, Mouchet, A, Najjar, RG, Plattner, G-K, Rodgers, KB, Sabine, CL, Sarmiento, JL, Schlitzer, R, Slater, RD, Totterdell, IJ, Weirig, M-F, Yamanaka, Y and **Yool, A.** 2005. Anthropogenic ocean acidification over the twenty-first century and its impact on calcifying organisms. *Nature* **437**: 681–686. DOI: https://doi.org/10.1038/nature04095

Pelletier, G, Roberts, M, Keyzers, M and **Alin, SR.** 2018. Seasonal variation in aragonite saturation in surface waters of Puget Sound – a pilot study. *Elem Sci Anth* **6**(1). DOI: https://doi.org/10.1525/elementa.270

Persson, E. 2018. A comparison between short-term sediment traps with filtered sea water and without during two contrasting periods with respect to Chl a and phytoplankton composition. Bachelor thesis, UiT- The Arctic University of Norway.

Redfield, AC, Ketchum, BH and **Richards, FA.** 1963. The influence of organisms on the composition of seawater. Hill, MN (ed.), *The Sea: Ideas and Observations on the Progress in the Study of the Seas* **2**: 26–77. New York: Interscience.

Register of Aquaculture Permissions. 2018. *Fiskerdirectoratet*. Available from: https://register.fiskeridir.no/akvareg/?loknr=13804.

Reigstad, M and **Wassmann, P.** 1996. Importance of advection for pelagic-benthic coupling in north Norwegian fjords. *Sarsia* **80**(4): 245–257. DOI: https://doi.org/10.1080/00364827.1996.10413599

Reisdorph, SC and **Mathis, JT.** 2014. The dynamic controls on carbonate mineral saturation states and ocean acidification in a glacially dominated estuary. *Estuar Coast Shelf Sci* **144**: 8–18. DOI: https://doi.org/10.1016/j.ecss.2014.03.018

Rost, B and **Riebesell, U.** 2004. Coccolithophores and the biological pump: responses to environmental changes. In: *Coccolithophores*. Thierstein, HR and Young, JR (eds.), 99–125. Berlin, Heidelberg: Springer. DOI: https://doi.org/10.1007/978-3-662-06278-4_5

Rysgaard, S, Mortensen, J, Juul-Pedersen, T, Sørensen, LL, Lennert, K, Søgaard, DH, Arendt, KE, Blicher, ME, Sejr, MK and **Bendtsen, J.** 2012. High air–sea CO_2 uptake rates in nearshore and shelf areas of Southern Greenland: temporal and spatial variability. *Mar Chem* **128–129**: 26–33 DOI: https://doi.org/10.1016/j.marchem.2011.11.002

Sætre, R. 2007. The Norwegian Coastal Current: Oceanography and Climate. Trondheim: Fagbokforlaget. ISBN: 978-82-519-2184-8.

Salvanes, AGV and **Noreide, JT.** 1993. Dominating sublittoral fish species in a west Norwegian fjord and their trophic links to cod (*Gadus morhua* L.). *Sarsia* **78**(3–4): 221–234. DOI: https://doi.org/10.1080/00364827.1993.10413536

Sambrotto, RN, Savidge, G, Robinson, C, Boyd, P, Takahashi, T, Karl, DM, Langdon, C, Chipman, D, Marra, J and **Codispoti, L.** 1993. Elevated consumption of carbon relative to nitrogen in the surface ocean. *Nature* **363**: 248–250. DOI: https://doi.org/10.1038/363248a0

Shadwick, EH, Thomas, H, Chierici, M, Else, B, Fransson, A, Michel, C, Miller, LA, Mucci, A, Niemi, A, Papakyriakou, TN and **Tremblay, J-É.** 2011. Seasonal variability of the organic carbon system in the Amundsen Gulf region of the southeastern Beaufort Sea. *Limnol Oceanogr* **56**(1): 303–322. DOI: https://doi.org/10.4319/lo.2011.56.1.0303

Signorini, SR, Mannino, A, Najjar, RG, Friedrichs, MAM, Cai, W-J, Salisbury, J, Wang, ZA, Thomas, H and **Shadwick, E.** 2013. Surface ocean pCO_2 seasonality and sea-air CO_2 flux estimates for the North American east coast. *J Geophys Res Ocean* **118**: 5439–5460. DOI: https://doi.org/10.1002/jgrc.20369

Skarðhamar, J and **Svendsen, H.** 2005. Circulation and shelf-ocean interaction off North Norway. *Cont Shelf Res* **25**(12–13): 1541–1560. DOI: https://doi.org/10.1016/j.csr.2005.04.007

Smith, RW, Bianchi, TS, Allison, M, Savage, C and **Galy, V.** 2015. High rates of organic carbon burial in fjord sediments globally. *Nature Geosci* **8**: 450–453. DOI: https://doi.org/10.1038/ngeo2421

Spall, MA, Jackson, RH and **Straneo, F.** 2017. Katabatic wind-driven exchange in fjords. *J Geophys Res Oceans* **122**(10): 8246–8262. DOI: https://doi.org/10.1002/2017JC013026

Syvitski, JPM, Burrell, DC and **Skei, JM.** 1987. Fjords: Processes and Products. *Springer Science & Business Media*. ISBN: 978-1-4612-4632-9. DOI: https://doi.org/10.1007/978-1-4612-4632-9

Takahashi, T, Olafsson, J, Goddard, JG, Chipman, DW and **Sutherland, SC.** 1993. Seasonal variation of CO_2 and nutrients in the high-latitude surface oceans: A comparative study. *Glob Biogeochem Cy* **7**(4): 843–878. DOI: https://doi.org/10.1029/93GB02263

Takahashi, T, Sutherland, SC, Sweeney, C, Poisson, A, Metzl, N, Tillbrook, B, Bates, N, Wanninkhof, R, Feely, RA, Sabine, C, Olafsson, J and **Nojiri, Y.** 2002. Global sea–air CO_2 flux based on climatological surface ocean pCO_2, and seasonal biological and temperature effects. *Deep Sea Res II* **49**: 1601–1622. DOI: https://doi.org/10.1016/S0967-0645(02)00003-6

Takahashi, T, Sutherland, SC, Wanninkhof, R, Sweeney, C, Feely, RA, Chipman, DW, Hales, B, Friederich, G, Chavez, F, Sabine, C, Watson, A, Bakker, DCE, Schuster, U, Metzl, N, Yoshikawa-Inoue, H, Ishii, M, Midorikawa, T, Nojiri, Y, Körtzinger, A, Steinhoff, T, Hoppema, M, Olafsson, J, Arnarson, TS, Tilbrook, B, Johannessen, T, Olsen, A, Bellerby, R, Wong, CS, Delille, B, Bates, NR and **de Baar, HJW.** 2009. Climatological mean and decadal change in surface ocean pCO_2, and net sea–air CO_2 flux over the global oceans. *Deep Sea Res II* **56**: 554–577. DOI: https://doi.org/10.1016/j.dsr2.2008.12.009

Takeda, S. 1998. Influence of iron availability on nutrient consumption ratio of diatoms in oceanic waters. *Nature* **393**: 774–777. DOI: https://doi.org/10.1038/31674

Thomas, H, Bozec, Y, Elkalay, K and **de Baar, HJW.** 2004. Enhanced open ocean storage of CO_2 from shelf sea pumping. *Science* **304**: 1005–1008. DOI: https://doi.org/10.1126/science.1095491

Thomas, H and **Schneider, B.** 1999. The seasonal cycle of carbon dioxide in Baltic Sea surface waters. *J Marine Syst* **22**: 53–67. DOI: https://doi.org/10.1016/S0924-7963(99)00030-5

Thomas, H, Schiettecatte, L-S, Suykens, K, Koné, YJM, Shadwick, EH, Prowe, AEF, Bozec, Y, de Baar, HJW and **Borges, AV.** 2009. Enhanced ocean carbon storage from anaerobic alkalinity generation in coastal sediments. *Biogeosci* **6**: 267–274. DOI: https://doi.org/10.5194/bg-6-267-2009

Tremblay, J-É, Simpson, K, Martin, J, Miller, L, Gratton, Y, Barber, D and **Price, NM.** 2008. Vertical stability and the annual dynamics of nutrients and chlorophyll fluorescence in the coastal, southeast Beaufort Sea. *J Geophys Res Oceans* **113**(C7): C07S90. DOI: https://doi.org/10.1029/2007JC004547

Turk, D, Bedard, JM, Burt, WJ, Vagle, S, Thomas, H, Azetsu-Scott, K, McGillis, WR, Iverson, SJ and **Wallace, DWR.** 2016. Inorganic carbon in a high latitude estuary-fjord system in Canada's eastern Arctic. *Estuar Coast Shelf Sci* **178**: 137–147. DOI: https://doi.org/10.1016/j.ecss.2016.06.006

Tynan, E, Clarke, JS, Humphreys, MP, Ribas-Ribas, M, Esposito, M, Rérolle, VMC, Schlosser, C, Thorpe, SE, Tyrrell, T and **Achterberg, EP.** 2016. Physical and biogeochemical controls on the variability in surface pH and calcium carbonate saturation states in the Atlantic sectors of the Arctic and Southern Oceans. *Deep Sea Res II* **127**: 7–27. DOI: https://doi.org/10.1016/j.dsr2.2016.01.001

Tyrrell, T, Holligan, PM and **Mobley, CD.** 1999. Optical impacts of oceanic coccolithophore blooms. *J Geophys Res* **104**(C2): 3223–3241. DOI: https://doi.org/10.1029/1998JC900052

van Heuven, S, Pierrot, D, Rae, JWB, Lewis, E and **Wallace, DWR.** 2011. MATLAB program developed for CO_2 system calculations. *ORNL/CDIAC-105b*. Oak Ridge, TN: Carbon Dioxide Information Analysis Center, Oak Ridge National Laboratory, US Department of Energy, Oakridge, Tennessee. DOI: https://doi.org/10.3334/CDIAC/otg.CO2SYS_MATLAB_v1.1

Vaquer-Sunyer, R, Duarte, CM, Holding, J, Regaudie-de-Gioux, A, García-Corral, LS, Reigstad, M and **Wassman, P.** 2013. Seasonal patterns in Arctic planktonic metabolism (Fram Strait–Svalbard region). *Biogeosci* **10**: 1451–1469. DOI: https://doi.org/10.5194/bg-10-1451-2013

Walker, E-Z. 2018. Pelagic-benthic coupling in a northern Norwegian fjord over winter: considering seasonality in high-latitude aquaculture. Masters thesis, Iceland: University of Akureyri, University Centre of the Westfjords, 76 pp.

Wanninkhof, R. 2014. Relationship between wind speed and gas exchange over the ocean revisited. *Limnol Oceanogr Methods* **12**(6): 351–362. DOI: https://doi.org/10.4319/lom.2014.12.351

Wassmann, P, Peinert, R and **Smetacek, V.** 1991. Patterns of production and sedimentation in the boreal and polar Northeast Atlantic. *Polar Res* **10**(1): 209–228. DOI: https://doi.org/10.3402/polar.v10i1.6740

Weiss, RF. 1974. Carbon dioxide in water and seawater: The solubility of a non-ideal gas. *Mar Chem* **2**: 203–215. DOI: https://doi.org/10.1016/0304-4203(74)90015-2

Wiedmann, I, Reigstad, M, Marquardt, M, Vader, A and **Gabrielsen, TM.** 2016. Seasonality of vertical flux and sinking particle characteristics in an ice-free high arctic fjord—Different from subarctic fjords? *J Mar Sys* **154**(Part B): 192–205. DOI: https://doi.org/10.1016/j.jmarsys.2015.10.003

Woosley, RJ, Millero, FJ and **Takahashi, T.** 2017. Internal consistency of the inorganic carbon system in the

Arctic Ocean. *Limnol Ocean Methods* **15**: 887–896. DOI: https://doi.org/10.1002/lom3.10208

Yamamoto-Kawai, M, McLaughlin, FA, Carmack, EC, Nishino, S and **Shimada, K.** 2009. Aragonite undersaturation in the Arctic Ocean: Effects of ocean acidification and sea ice melt. *Science* **326**: 1098–1100. DOI: https://doi.org/10.1126/science.1174190

Yasunaka, S, Murata, A, Watanabe, E, Chierici, M, Fransson, A, van Heuven, S, Hoppema, M, Ishii, M, Johannessen, T, Kosugi, N, Lauvset, SK, Mathis, JT, Nishino, S, Omar, AM, Olsen, A, Sasano, D, Takahashi, T and **Wanninkhof, R.** 2016. Mapping of the air–sea CO_2 flux in the Arctic Ocean and its adjacent seas: Basin-wide distribution and seasonal to interannual variability. *Polar Sci* **10**: 323–334. DOI: https://doi.org/10.1016/j.polar.2016.03.006

Zeebe, RE and **Wolf-Gladrow, D.** 2001. CO_2 in Seawater: Equilibrium, Kinetics, Isotopes. Amsterdam: Elsevier, 346.

How to cite this article: Jones, EM, Renner, AHH, Chierici, M, Wiedmann, I, Lødemel, HH and Biuw, M. 2020. Seasonal dynamics of carbonate chemistry, nutrients and CO_2 uptake in a sub-Arctic fjord. *Elem Sci Anth*, 8: 41. DOI: https://doi.org/10.1525/elementa.438

Domain Editor-in-Chief: Jody W. Deming, School of Oceanography, University of Washington, US

Associate Editor: Lisa A. Miller, Institute of Ocean Sciences, Fisheries and Oceans Canada, CA

Knowledge Domain: Ocean Science

Part of an *Elementa* Special Feature: Advances in Ocean Acidification Research

Submitted: 26 January 2020 **Accepted:** 10 July 2020 **Published:** 17 August 2020

ELEMENTA Science of the Anthropocene

Elem Sci Anth is a peer-reviewed open access journal published by University of California Press.

OPEN ACCESS